Asymmetrical localization of components of the Nup107-160 subcomplex within the nuclear pore complex in fission yeast

Haruhiko Asakawa[1], Tomoko Kojidani[2,3], Hui-Ju Yang[1], Chizuru Ohtsuki[1], Hiroko Osakada[2], Masaaki Iwamoto[2], Naomi Takagi[4], Koji Nagao[4,5], Chikashi Obuse[4,5], *Yasushi Hiraoka[1,2] & *Tokuko Haraguchi[1,2]

1 Graduate School of Frontier Biosciences, Osaka University, Suita, Japan

2 Advanced ICT Research Institute Kobe, National Institute of Information and Communications Technology, Kobe, Japan

3 Department of Chemical and Biological Sciences, Faculty of Science, Japan Women's University, Tokyo, Japan

4 Graduate School of Life Science, Hokkaido University, Sapporo, Japan.

5 Graduate School of Science, Osaka University, Toyonaka, Japan.

*Corresponding authors:

Tokuko Haraguchi

e-mail: tokuko@nict.go.jp

Yasushi Hiraoka

e-mail: hiraoka@fbs.osaka-u.ac.jp

Abstract

The nuclear pore complex (NPC) forms a gateway for nucleocytoplasmic transport. The NPC consists of several protein subcomplexes. Nup107-160 is a key subcomplex responsible for building the basal NPC structure by symmetrical localization on the nuclear and cytoplasmic sides of the nuclear pore. Here we found an unusual asymmetrical localization of the Nup107-160 subcomplex in fission yeast. Two disconnected/split pieces of the Nup107-160 subcomplex were differentially distributed to either side of the NPC, as revealed by immunoelectron microscopy and affinity-capture/mass spectrometry for nucleoporins. Nup131 and Nup132 (paralogs of human Nup133) were differentially localized on the cytoplasmic and nuclear sides, respectively. The expression of a fusion protein connecting the disrupted components of the Nup107-160 subcomplex caused symmetrical localization of Nup132, leading to defects in mitosis and meiosis. These observations suggest that the asymmetrical NPC structure is necessary for normal cell cycle progression in fission yeast.

Keywords: nuclear pore complex, nucleoporin, Nup133, Y-complex, immunoelectron microscopy, mass spectrometry

Introduction

In eukaryotes, the nuclear envelope (NE) separates the nucleus from the cytoplasm. Molecular transport between the nucleus and cytoplasm across the NE occurs through nuclear pore complexes (NPCs). These complexes are cylindrical, eight-fold symmetrical structures that perforate the NE and are made of multiple sets of about 30 different protein species known as nucleoporins (Nups) (Rout et al., 2000; Cronshaw et al., 2002; Alber et al., 2007). Nups are classified into three groups: transmembrane Nups, FG repeat Nups, and scaffold Nups. Transmembrane Nups have transmembrane motifs and anchor NPCs to the NE. FG repeat Nups contain phenylalanine-glycine (FG) rich repeats and are involved in molecular transport inside the NPC cylinder structure. Scaffold Nups form two inner rings and two outer rings, which serve as the NPC structural core, and associate with the membrane through interactions with transmembrane Nups (Bui et al., 2013; von Appen et al., 2015; Kosinski et al., 2016; Lin et al., 2016). These NPC structures and most nucleoporins are conserved among many eukaryotes (Rout et al., 2000; Cronshaw et al., 2002; DeGrasse et al., 2009; Tamura et al., 2010; Amlacher et al., 2011; Obado et al., 2016), although numerous species-dependent differences are found (Knockenhauer and Schwartz, 2016).

The Nup107-160 subcomplex is a key component of the outer rings and is composed of Nup107, Nup85, Nup96, Nup160, Nup133, Sec13, and Seh1 in most eukaryotes; depending on the species, Nup37, Nup43, and ELYS are also included (Walther et al., 2003; Harel et al., 2003; Loïodice et al., 2004; Rasala et al., 2006; Liu et al., 2009; Thierbach et al., 2013). These nucleoporins assemble to form the Y-shaped Nup107-160 subcomplex *in vitro* and/or *in vivo* in *Homo sapiens*, the budding yeast *Saccharomyces cerevisiae*, and the thermophile *Chaetomium thermophilum* (von Appen

et al., 2015; Thierbach et al., 2013; Kampmann and Blobel, 2009; Flemming et al., 2010; Fernandez-Martinez et al., 2012; Kelley et al., 2015; Stuwe et al., 2015). Nup85, Nup43, and Seh1 form one of the two short arms, while Nup160, Nup37, and ELYS form the other. The two arms are connected to Nup96 and Sec13, creating the three-pronged structure. Nup96 is connected to Nup107 and Nup133 to form the long stem (Nup96-Nup107-Nup133) of the Y-shaped molecule. Multiple copies of the Nup107-160 subcomplex form the outer rings on the nucleoplasmic and cytoplasmic sides of the NPC (Bui et al., 2013; von Appen et al., 2015; Kelley et al., 2015; Stuwe et al., 2015).

Like other eukaryotes, the fission yeast *Schizosaccharomyces pombe* has a set of conserved Nups (Baï et al., 2004; Chen et al., 2004; Asakawa et al., 2014). The *S. pombe* NPC contains spNup37 and spEly5, a potential homolog of metazoan ELYS, but not Nup43 (Asakawa et al., 2014; Bilokapic and Schwartz, 2012) (hereafter, we add the prefix 'sp' to denote *S. pombe* proteins). In addition, *S. pombe* carries several redundant Nups: two Nup133 and two scNic96/hsNup93 homologs, each (hereafter, sc and hs are used to indicate *S. cerevisiae* and *H. sapiens* proteins). The two Nup133 homologs in *S. pombe*, spNup131 (spNup133a) and spNup132 (spNup133b), are able to interact biochemically with spNup107 (Baï et al., 2004). Despite their similar biochemical features, spNup131 and spNup132 are likely to have different functions because gene disruption strains show different phenotypes; nup132Δ but not Nup131Δ display altered NPC distribution (Baï et al., 2004), and the strain lacking spNup132 (*nup132*Δ) but not that lacking spNup131 (*nup131*Δ) is inhibited for growth in the presence of a microtubule-depolymerizing drug (thiabendazole) or a DNA replication inhibitor (hydroxyurea) (Chen et al., 2004; Asakawa et al., 2014). In meiosis, *nup132*Δ but not

*nup131*Δ exhibits delayed chromosome segregation and unusual spore formation (Asakawa et al., 2014; Yang et al., 2015). In addition, telomere elongation and deficiency in SUMOylation have been reported in *nup132*Δ-specific phenotypes (Liu et al., 2010; Nie and Boddy, 2015). The causes of these functional differences remain unknown.

In the present study, we used immunoelectron microscopy to determine the localization of each Nup in *S. pombe* NPCs. To understand the overall structure of the *S. pombe* NPC, we performed interactome studies of Nups using affinity capture and mass spectrometry. Our results reveal a unique structure for the *S. pombe* Nup107-160 subcomplex and suggest that a variation in NPC organization developed during evolution.

Results

spNup131 and spNup132 are differently positioned at the cytoplasmic and nucleoplasmic sides of the NPC

The molecular architectures of spNup131 and spNup132 are similar, with an N-terminal β-propeller domain followed by a C-terminal α-helix stack domain in the C-terminus, as found in other species (Whittle and Schwartz, 2009) (**Figure 1a**). However, phylogenetic analysis indicates that spNup131 and spNup132 belong to evolutionarily distant clades, with the spNup131-containing clade branching from a common ancestor much earlier than that of spNup132 (**Figure 1–figure supplement 1**). This result suggests that despite the similarity in their domain architecture, spNup131 and spNup132 may have structural features that are distinct enough to confer different functions.

To investigate the differences between spNup131 and spNup132, we first determined the localization of these Nups within the NPC using immunoelectronmicroscopy (IEM) (see Materials and Methods for details). The spNup131 or spNup132 gene was replaced with the respective gene N-terminally fused to GFP (GFP-spNup131 or GFP-spNup132). The results showed that GFP-spNup131 is located at the cytoplasmic side of the NPC, while GFP-spNup132 is located at the nuclear side (**Figure 1b**). To confirm the accessibility of the nucleus to immunogold particles using this method, the nuclear centromere protein spMis6 (Saitoh et al., 1997) was co-stained (**Figure 1–figure supplement 2**); only the cells positive for spMis6 were evaluated for staining of spNup131. IEM to detect GFP-spNup131 in cells simultaneously expressing spMis6-GFP showed that spNup131 is localized only at the cytoplasmic side of the NPC (**Figure 1–figure supplement 2**). Montage pictures with quantification show the distribution of spNup131 and spNup132 and confirm the distinct locations of spNup131 and spNup132 in the NPC; spNup131 and spNup132 were exclusively located in the cytoplasmic and nuclear, respectively (**Figure 1c, Figure 1–figure supplement 2**). To consider potential artifacts of GFP-tagging at the N-terminus, we repeated these experiments using strains in which spNup131 or spNup132 was C-terminally fused to GFP and obtained essentially the same results (**Figure 1d**). These results indicate that spNup131 and spNup132 are differentially positioned at the cytoplasmic and nuclear sides, respectively, of the NPC.

Immunoelectron microscopy of spNup107-160 subcomplex Nups

Because the Nup133 homologs are integrated components of the Nup107-160 subcomplex, we next examined positioning of the other Nup107-160 subcomplex

components in *S. pombe*: spNup107 (scNup84/hsNup107), spNup120 (scNup120/hsNup160), spNup85 (scNup85/hsNup85), spNup96 (also known as spNup189C; scNup146C/hsNup96), spNup37 (hsNup37), spSeh1 (scSeh1/hsSeh1), and spEly5 (hsELYS) in the cells expressing each GFP-fused Nup as a sole component. The spNup98-spNup96 fusion protein is generated as the *nup189*$^{+}$ gene product, and spNup96 is separated by the peptides conferring autopeptidase activity in the C-terminus of spNup98 (also known as spNup189N) (Asakawa et al., 2015). The C-terminal tag on spNup96 does not inhibit separation of spNup98 from spNup96 (Asakawa et al., 2015).

Results of IEM show that of the 7 nucleoporins, spNup107 is located on the nuclear side of the NPC, whereas spNup120, spNup85, spNup96, spNup37, spEly5, and spSeh1 are predominantly located on the cytoplasmic side of the NPC (**Figure 2a**). The localization of spNup107 on the nuclear side was also confirmed using an N-terminus fusion protein (**Figure 2a**). Simultaneous detection of spMis6-GFP further confirmed the localization of spNup120, spNup96, spNup85, spNup37, spSeh1, and spEly5 on the cytoplasmic side (**Figure 2a**). This result suggests that the Nup107-160 subcomplex is disrupted into two pieces in *S. pombe* and that these two pieces are differentially located on the cytoplasmic and nuclear sides of the NPC.

Location of other Nups in the NPC

We also performed IEM of other Nups to reveal their locations within the NPC in *S. pombe* (**Figure 2b-f**). We first examined inner ring Nups known as the Nup93 subcomplex in vertebrates. spNup97 and spNpp106, redundant *S. pombe* homologs of scNic96/hsNup93, were both similarly positioned near the center of the NPC. spNup184

(scNup188/hsNup188) and spNup186 (scNup192/hsNup205) were also positioned near the center (**Figure 2b**). The redundancy of scNic96/hsNup93 homologs is unique in the *Schizosaccharomyces* genus (**Figure 2–figure supplement 1**). spNup40 and spNup155 were also located near the center of the NPC, but they showed a slightly broader range of localization (**Figure 2b**).

The channel Nups spNup44 (scNup57/hsNup54) and spNup45 (scNup49/hsNup58) were localized at the center of the pore (**Figure 2c**). spNup98 (scNup145n/hsNup98) was also found near the center of the pores when examined with an antibody against the N-terminal region (Iwamoto et al., 2013) (see "spNup98" in **Figure 2c**). The C-terminal region of spNup98 tagged with GFP was detected on the cytoplasmic side of the nuclear pore using an anti-GFP antibody (see "spNup98-GFP" in **Figure 2c**). In *H. sapiens* and *S. cerevisiae*, the C-terminal region of the Nup98 homologs (hsNup98/scNup145n/scNup100/scNup116) interacts with Nup96 homologs (hsNup96/scNup145c) (Hodel et al., 2002; Griffis et al., 2003; Ratner et al., 2007). In addition, the C-terminal mouse Nup98-APD (autoproteolytic and NPC-targeting domain) binds the conserved cytoplasmic scNup82 (Stuwe et al., 2012). Thus, the C-terminal region of spNup98 might be tethered by spNup96 and spNup82, both of which are positioned at the cytoplasmic side of the NPC, while the N-terminal region is extended to the center of the pore. *S. pombe* homologs of the conserved Nup Nsp1 (scNsp1/hsNup62) was localized frequently in the cytoplasmic side and infrequently in the nuclear side of the NPC (**Figure 2d**). The conserved cytoplasmic Nups spNup82 (scNup82/hsNup88) and spNup146 (scNup159/hsNup214) also localized to the cytoplasmic side (**Figure 2e**). The conserved nuclear Nups spNup61 (scNup2/hsNup50), spNup124 (scNup1/hsNup153), spNup211 (scMlp1/scMlp2/hsTpr), and spNup60

(scNup60) were localized at the nuclear side (**Figure 2f**). The transmembrane Nups spCut11 (scNdc1/hsNdc1), spPom152 (scPom152), and spPom34 (scPom34) were localized at the center of the pore and slightly biased toward the cytoplasm (**Figure 2g**).

Interaction mapping of *S. pombe* Nups

To understand the overall structure of the *S. pombe* NPC, which is likely assembled with the unusual characteristics as described above, we performed affinity capture/mass spectrometry of *S. pombe* nucleoporins. Whole cell extracts were prepared from *S. pombe* strains expressing each of the GFP-fused nucleoporins from the endogenous genomic locus and subjected to immunoprecipitation with anti-GFP antibodies (see Materials and Methods for details). Proteins precipitated with GFP-nucleoporins were separated on SDS polyacrylamide gels and analyzed by liquid chromatography coupled to tandem mass spectrometry (LC/MS/MS) (**Figure 3–figure supplement 1**). The abundance of immunoprecipitated nucleoporins was semi-quantified using emPAI (exponentially modified protein abundance index) values (Ishihama et al., 2005), yielding a map of the interactions between *S. pombe* nucleoporins (**Figure 3**).

We first focused on proteins interacting with components of the Nup107-160 subcomplex. spNup107 co-precipitated with spNup132 and vice versa, which is consistent with the previous study (Baï et al, 2004), suggesting that they form a complex *in vivo* in analogy to eukaryotic homologs (e.g., scNup84-133 and hsNup107-133). However, in contrast to studies in humans and *S. cerevisiae*, spNup107 did not effectively interact with spNup96, a result consistent with IEM data showing separate locations of spNup107 and spNup96 at the nuclear and cytoplasmic sides of the NPC, respectively. spNup107 co-precipitated spNup131, suggesting these proteins

interact with each other only when they are together in cell extracts, as the IEM data showed that spNup107 and spNup131 were located on different sides of the NPC. Because immunoprecipitation does not ensure direct interaction between the two components, we performed yeast two-hybrid assays to investigate the direct binding ability between any two components of the Nup107-160 subcomplex. spNup107 bound spNup132 but not spNup131 (**Figure 4a**), consistent with IEM data indicating that spNup107 and spNup132 but not spNup131 are located on the nuclear side of the NPC. No or minimal interaction was detected between spNup107 and spNup96 (**Figure 4a**), suggesting a separation between spNup107 and spNup96, as found in IEM and affinity capture/mass spectrometry analyses. spNup96 bound to spNup85 (**Figure 4a**); spNup96 bound to spNup120 in the presence of spNup85 (**Figure 4b**); spSeh1 bound to spNup85 (**Figure 4c**); spNup37 bound to spNup120 (**Figure 4c**); spEly5 bound to spNup120 in the presence of spNup37 but not in the absence of spNup37 (**Figure 4d**); and spNup37 and spEly5 did not interact with each other (**Figure 4e**). These results suggest that spNup120–spNus37–spEly5, spNup85–spSeh1, and spNup96 form a complex, as suggested by IEM and affinity capture/mass spectrometry analyses in this study and previous studies (Bilokapic et al., 2012). The Nup37-dependent interaction of ELYS with Nup120 is also reported for *C. thermophilum* (Thierbach et al., 2013). These results support the idea that in the Nup107-160 subcomplex, the protein complex containing spNup96 and the other complex containing spNup107 are in separate locations in *S. pombe*, as indicated by IEM.

Interaction and/or complex formation between other Nups was also examined by LC/MS/MS analysis of affinity-captured Nups. The results suggest a modular organization of *S. pombe* NPC subcomplexes, including the Nup93 subcomplex

(spNup97, spNpp106, spNup184, spNup186, spNup155, and spNup40), channel Nup subcomplex (spNup45, spNup44 and spNsp1), cytoplasmic ring complex (spNsp1, spNup82 and spNup146), nuclear basket Nups (spNup211, spNup60, spNup61, and spNup124) and transmembrane Nups (spCut11, spPom152, and spPom34) (**Figure 3**). In the *S. pombe* Nup93 subcomplex, the redundant Nups spNpp106 and spNup97 showed different affinities toward spNup184 and spNup186: spNup97 preferentially interacted with spNup186, while spNpp106 preferentially interacted with spNup184 (**Figure 3**). The Nup93 subcomplex Nups interacted with channel Nups, and vice versa (**Figure 3**). Because an interaction of the Nup93 subcomplex and the channel Nup complex has been reported previously in *S. cerevisiae* and *C. thermophilum* (Amlacher et al., 2011; Stuwe et al., 2015; Fischer et al., 2015), our result suggests that the interaction between these two subcomplexes is also conserved in *S. pombe*. In addition to the interaction with the channel Nups subcomplex, the Nup93 subcomplex interacts with transmembrane Nups (**Figure 3**). Interestingly, spNup155 in the Nup93 subcomplex co-precipitated many Nups, including some of the Nup107-160 subcomplex Nups, channel Nup spNup44, and transmembrane Nups, suggesting that spNup155 may play a role in connecting many subcomplexes/modules of the NPC in *S. pombe* (**Figure 3**). Taken together, these results suggest that the *S. pombe* NPC exhibits a split organization of the Nup107-160 subcomplex, and this unique structure may be maintained by evolutionarily conserved subcomplexes and their mutual interactions.

The position of each subcomplex and Nup within the NPC in *S. pombe* was summarized based on the results from immunoelectron microscopy, affinity capture/mass spectrometry, and yeast two-hybrid assays in **Figure 5**.

The N-terminal β-propeller region is required for differential localization of Nup133 homologs

Next, we sought to determine which domains of spNup131 and spNup132 are responsible for their different localizations. In this experiment, we expressed fragments of spNup131 or spNup132 in a *nup131*Δ *nup132*Δ double-deletion strain (lacking genes for spNup131 and spNup132) to exclude the possibility that endogenous spNup131 or spNup132 predominantly occupies preferable sites for spNup131 and spNup132 fragments (**Figure 6a**). In the background of *nup131*Δ *nup132*Δ, the full-length spNup131 (spNup131FL) and spNup132 (spNup132FL) proteins tagged with GFP were localized at the nuclear periphery by fluorescence microscopy (FM) (**Figure 6b**). IEM revealed that GFP-spNup131 was localized at the cytoplasmic side of the NPC, while GFP-spNup132 localized at the nuclear side, consistent with the wild type strain (**Figure 6c**). This result suggests that spNup131 and spNup132 were localized to their proper sites independent of each other, and that they cannot substitute for one another. FM analysis revealed that the C-terminal region (spNup132C) but not the N-terminal region (spNup132N) was localized to the nuclear periphery (**Figure 6b**). IEM analysis revealed localization of spNup132C on the nuclear side of the NPC (**Figure 6c**). The spNup131 C-terminal region (spNup131C) but not the N-terminal region (spNup131N) was localized at the nuclear periphery, as with spNup132. However, surprisingly, IEM analysis revealed that spNup131C is positioned at the nuclear side of the NPC, in contrast to the full-length protein, which localized on the cytoplasmic side. This indicates that the N-terminal β-propeller domain of spNup131 is required for the proper localization of this protein to the cytoplasmic side.

To understand which domains of spNup131 and spNup132 are responsible for

283 their interactions with spNup107, we carried out yeast two-hybrid assays (**Figure 6d**).
284 The results showed that the C-terminal region of spNup131 but not the full-length
285 protein bound to spNup107 (**Figure 6d**). In contrast, both the spNup132 C-terminal
286 region and the full-length protein bound to spNup107 (**Figure 6d**). Thus, these results
287 suggest that the C-terminal regions of both spNup131 and spNup132 have the potential
288 to interact with spNup107 and that the N-terminal region of spNup131 plays a role in
289 preventing interaction with spNup107. Taken together, we conclude that the N-terminal
290 region of spNup131 is necessary but not sufficient for the cytoplasmic localization of
291 spNup131.
292
293 **Forced symmetrical localization of spNup132 causes defects in normal cell cycle**
294 **progression**
295 To address the significance of the separation of the *S. pombe* Nup107-160 subcomplex,
296 we generated an *S. pombe* strain with spNup96 artificially fused to spNup107 in the
297 *nup107*Δ background (spNup96-spNup107-GFP). The strain was viable, and Western
298 blot analysis confirmed expression of the protein with the predicted molecular weight
299 (**Figure 7a**). By IEM, the majority of the spNup96-spNup107-GFP fusion protein
300 molecules were localized at the cytoplasmic side of the NPC (**Figure 7b**), a change in
301 the location of spNup107 from the nuclear side to the cytoplasmic side. Under this
302 condition, spNup132 was recruited to both the nuclear and cytoplasmic sides of the
303 NPC (**Figure 7c**), suggesting that a fraction of the spNup132 molecules was recruited
304 by spNup107. Next, we examined the phenotype of the strain expressing the
305 spNup96-spNup107-GFP fusion protein. This strain exhibited growth sensitivity to the
306 microtubule-destabilizing drug thiabendazole (TBZ) (**Figure 7d)**, delayed meiotic

division (**Figure 7e, f**), and abnormal spore formation (**Figure 7g**) as previously reported for *nup132*Δ cells (Chen et al., 2004; Asakawa et al., 2014; Yang et al., 2015). This result suggests that the split structure and the asymmetrical localization in the Nup107-160 subcomplex are necessary for retaining Nup132 at the nuclear side of the NPC, which in turn is necessary for normal progression of mitosis and meiosis in *S. pombe*.

Function of spNup131 at the cytoplasmic side of the NPC

To determine the function of spNup131, we next examined its interacting proteins. Affinity capture/mass spectrometry identified several proteins other than Nups that interact with spNup131 (**Supplementary File 1**). Among these proteins, we searched for those that localize at the nuclear periphery and found spFar8 (also known as spCsc3). This protein is one of the components of the striatin-interacting phosphatase and kinase (STRIPAK) complex (Goudreault et al., 2009; Frost et al., 2012) that regulates the functions of the spindle pole body (SPB; equivalent of MTOC) during mitosis (Singh et al., 2011). GFP-fused spFar8 (spFar8-GFP) localized at the nuclear periphery during interphase, as previously reported (Singh et al., 2011) (see "wild type" in **Figure 8a**). To test whether localization of spFar8 at the nuclear periphery depends on the NPC, we examined the location of spFar8-GFP in the background of *nup132*Δ. It is known that NPCs have a clustered distribution on the NE in the background of *nup132*Δ (Baï et al., 2004; Asakawa et al., 2014). spFar8-GFP exhibited the clustered distribution with NPCs labeled with spCut11(scNdc1/hsNdc1)-mCherry in *nup132*Δ cells (**Figure 8b**). In addition, the localization of spFar8 at the nuclear periphery greatly decreased in the background of *nup131*Δ (see "*nup131*Δ" in **Figure 8a**) despite no marked change in the

amount of spFar8 protein (**Figure 8c**). The localization of another STRIPAK complex protein, spFar11, to the nuclear periphery was also lower in *nup131*Δ cells (**Figure 8d**). These results suggest that spNup131 plays a role in retaining the STRIPAK complex at the NPC in interphase cells.

Discussion

IEM and yeast two-hybrid analyses of the *S. pombe* Nups suggest that the *S. pombe*-specific Nup107-160 subcomplex structure is uniquely split into two portions that localize differently to the cytoplasmic and nuclear sides of the NPC while preserving the conserved modular structures (**Figure 5**). In addition, affinity-capture/mass spectrometry analysis also partly supports this result (**Figure 3**). This specificity contrasts with the localization of the Nup107-160 subcomplexes in *H. sapiens*, *S. cerevisiae*, and *Trypanosoma brucei* in which the complex is found on both the cytoplasmic and nuclear sides of the NPC (Rout et al., 2000; Obado et al., 2016; D'Angelo et al., 2006). Our results suggest that the *S. pombe* NPC has a novel organization that has evolved in the *Schizosaccharomyces* genus, which commonly bears the Nup132 and Nup131 clades (**Figure 1–figure supplement 1**).

In *H. sapiens* and *S. cerevisiae*, the Nups in the Nup107-160 subcomplex assemble to form Y-shaped structures (Lutzmann et al., 2002; Kampmann and Blobel, 2009; Kelley et al., 2015; Stuwe et al., 2015; von Appen et al., 2015). A total of 32 Y-complexes form two concentric reticulated rings at both the nuclear and cytoplasmic side of the human NPC (Kelley et al., 2015; Stuwe et al., 2015; von Appen et al., 2015). This organization may be supported by the iso-stoichiometry of each Nup in the Nup107-160 subcomplex. In fact, the amounts of each Nup in the Nup107-160

355 subcomplex in human cells are nearly equal (Ori et al., 2013). In contrast, in *S. pombe*,
356 Sec13 and Nup43 are not present in the Nup107-160 subcomplex (Asakawa et al., 2014).
357 Furthermore, Nups of the Nup107-160 subcomplex are not iso-stoichiometrical, as
358 revealed in our previous study (Asakawa et al., 2014). The different composition and
359 stoichiometry of the *S. pombe* Nup107-160 subcomplex components is consistent with
360 the unique fission-yeast–specific separated structure of the Nup107-160 subcomplex
361 revealed in this study.

362 The role of the separate locations of the Nup107-160 subcomplex remains
363 unknown. In mammalian cells undergoing 'open mitosis,' the Nup107-160 subcomplex
364 is required for NPC assembly at an early stage of telophase and is therefore thought to
365 provide a structural element important for reconstructing the NPC at the end of mitosis
366 (Walther et al., 2003; Harel et al., 2003; Boehmer et al., 2003). Thus, the Nup107-160
367 subcomplex has essential scaffold functions. In contrast, Nup133 homologs are
368 dispensable for vegetative cell growth in fungi undergoing 'closed mitosis,' including *S.*
369 *pombe and S. cerevisiae* (Asakawa et al., 2014), suggesting a different role for Nup133
370 homologs among eukaryotes depending on the type of mitosis. While the role of
371 Nup133 homologs in vegetative cell growth in fungi is unknown, it is clear that
372 spNup132 but not spNup131 is required for the progression of meiosis in *S. pombe*,
373 especially with regard to proper segregation of meiotic chromosomes (Asakawa et al.,
374 2014; Yang et al., 2015). Such functional differences between spNup131 and spNup132
375 are reflected by the different locations of these two components within the NPC (**Figure**
376 **1**). A decrease in spNup132 on the nuclear side and its relocation to the cytoplasmic side
377 causes defects in meiosis similar to those found in *nup132Δ* cells, further supporting our
378 conclusion.

spNup132 is required for normal kinetochore formation during meiosis in *S. pombe*. Deletion of the *nup132* gene but not the *nup131* gene causes a delay in kinetochore protein assembly during the first meiotic chromosome segregation (Yang et al., 2015) and increases the sensitivity to a microtubule destabilizing drug, likely due to defects in the kinetochore structure (Asakawa et al., 2014). However, the molecular mechanism of underlying spNup132-mediated regulation of kinetochore proteins remains unknown. Similarly, in mammalian cells, kinetochore-related functions have been reported for the Nup107-160 subcomplex. A fraction of the Nup107-160 subcomplex is found at the kinetochores and spindle poles during mitosis (Harel et al., 2003; Loïodice et al., 2004; Belgareh et al., 2001; Orjalo et al., 2006), and depletion of the Nup107-160 subcomplex from kinetochores results in altered kinetochore protein recruitment (Zuccolo et al., 2007; Platani et al., 2009; Mishra et al., 2010). Considering the similarity in kinetochore-related functions, spNup132 but not spNup131 is likely to be a functional homolog of mammalian Nup133.

IEM analysis in this study revealed that spNup131 is localized only on the cytoplasmic side of the NPC. What is its function there? Our study revealed an interaction between spNup131 and spFar8. spFar8 is an *S. pombe* ortholog of the STRIPAK complex component Striatin (Frost et al., 2012) and is located at the nuclear periphery in interphase cells (Singh et al., 2011). In *S. pombe*, the STRIPAK complex regulates the septation initiation network through the conserved protein kinase Mob1 (Moreno et al., 2001; Goudreault et al., 2009) and is required for asymmetric division of mother and daughter SPBs during mitosis (Singh et al., 2011). The spNup131-dependent NPC localization of spFar8 revealed by this study implies that the NPC regulates STRIPAK localization in interphase cells. Human STRIPAK complexes

have been proposed to play roles at the interface between the Golgi and the outer nuclear envelope (Frost et al., 2012). Considering the localization of spNup131, STRIPAK is likely to interact with the NPC on the cytoplasmic side of the NE. Although the role of the STRIPAK complex in interphase cells in *S. pombe* is not fully understood, the interaction between spNup131 and spFar8 may provide an important example linking the NPC to cytoplasmic structures.

This study suggests that the *S. pombe* NPC maintains conserved modular structures while exhibiting some structural differences. In particular, the Nup107-160 subcomplex appears to have a novel separated structure and exhibits a localization pattern not reported in other organisms. Recent studies suggest that NPC structures are not necessarily the same among eukaryotes. For example, the binucleated ciliate *Tetrahymena thermophila* has two functionally distinct nuclei called the macronucleus (MAC) and micronucleus (MIC), which differ in size, transcriptional activity, and nucleocytoplasmic transport specificity (Karrer, 2012). Interestingly, in *T. thermophila,* the NPCs in the MAC and the MIC differ in the amount of Nup107-160 subcomplex present (Iwamoto et al., 2017). The amount of the subcomplex in the MIC is about three times more than that in the MAC, suggesting that the Nup107-160 subcomplex form different structures in the MAC and MIC. In addition, in some multicellular organisms, the expression level of Nups varies between cell types and during development (Ori et al., 2013; Cho et al., 2009; Olsson et al., 2004; D'Angelo et al., 2009; D'Angelo et al., 2012). It is also known that some mutations in Nups result in developmental defects in metazoans (Raices and D'Angelo, 2012). These findings suggest that the NPC composition in cell types and during development is biologically significant. An altered composition might alter the NPC structure, at least in part; thus, unidentified NPC

427 subcomplex structures may play roles in biological events. Thus, novel NPC structures
428 may be found in organisms or cell types with different compositions of Nups as we
429 found in *S. pombe*.
430

Materials and Methods

S. pombe strains and cultivation

The *S. pombe* strains used in this study are listed in supplementary Table 2. Fusion genes were constructed using a two-step PCR method and introduced into cells. YES or EMM2 culture medium was used for routine cultures (Moreno et al., 1991). ME medium was used to induce meiosis and spore formation. When necessary, TBZ was added to the YES medium to a final concentration of 10 μg/mL.

Immunoelectron microscopy

For immunoelectron microscopy, 1.5×10^8 cells were fixed in 1 mL of a mixture of 4% formaldehyde and 0.01% glutaraldehyde dissolved in 0.1 M phosphate buffer (PB) (pH7.4) for 20 min at room temperature, treated with 0.5 mg/mL Zymolyase 100T (Nacalai Tesque, Inc., Kyoto, Japan) in PB for 20-30 min at 30°C, and then permeabilized with 0.2% saponin (Nacalai Tesque, Inc.) and 1% bovine serum albumin (BSA) in PB for 15 min. The GFP epitope tag was labeled with a primary antibody (rabbit polyclonal anti-GFP antibody, Rockland Immunochemicals, Limerick, PA, USA) diluted at 1:400 in PB containing 1% BSA and 0.01% saponin, and a secondary antibody (goat anti-rabbit Alexa 594 FluoroNanogold Fab' fragment; Nanoprobes Inc., Yaphank, NY, USA) diluted 1:400. For analysis of the spNup98 N-terminal region, we used a mouse monoclonal anti-Nup98 antibody (13C2) (Iwamoto et al., 2013; Asakawa et al., 2015) diluted 1:100 and anti-mouse Alexa594 FluoroNanogold Fab' fragment (Nanoprobes) diluted 1:400. Cells then were fixed again with 1% glutaraldehyde in PB for 1 h at room temperature and treated with 100 mM lysine HCl in PB twice for 10 min each. The cells were stored at 4°C until use. Before use, the cells were incubated with

455 50 mM HEPES (pH 5.8) three times for 3 min each and with distilled water (DW) once,
456 incubated with the Silver enhancement reagent (a mixture of equal volumes of the
457 following A, B, and C solutions: A, 0.2% silver acetate solution; B, 2.8% trisodium
458 citrate-2H_2O, 3% citric acid-H_2O, and 0.5% hydroquinone; C, 300 mM HEPES, pH 8.2)
459 at 25°C for 3 min. Cells were embedded in 2% low melting agarose dissolved in DW.
460 Cells were post-fixed with 2% OsO_4 in DW for 15 min and stained with 1% uranyl
461 acetate in DW at room temperature. Cells were dehydrated using stepwise incubations
462 in ethanol and acetone and finally embedded in epoxy resin Epon812. Solidified blocks
463 containing cells were sectioned, and the ultra-thin sections were stained with uranyl
464 acetate and lead citrate, the usual pretreatment for EM observations. Images were
465 obtained using a JEM1400 transmission electron microscope (JEOL, Tokyo, Japan) at
466 120kV.
467 Nuclear pores containing more than two immunogold particles were chosen for
468 localization analysis as described previously (Rout et al., 2000). To confirm the
469 accessibility of the nucleus to immunogold particles, the nuclear centromere protein
470 spMis6-GFP was co-expressed with GFP-fused Nups in cells and stained with anti-GFP
471 antibody for IEM. For quantification of the Nup signals, we chose only cell specimens
472 with a positive spMis6-GFP signal. For quantitative representations, montage pictures
473 were produced by stacking 20 NPC images with 5% opacity on Adobe Photoshop CS
474 software.
475
476 ***cDNA clones***
477 *nup107*$^+$ and *nup37*$^+$ cDNAs were provided by National BioResource Project Japan
478 (http://yeast.lab.nig.ac.jp/yeast/top.xhtml). cDNA fragments of other Nups were

amplified from a cDNA library pTN-RC5 or pTN-FC9 (National BioResource Project Japan) using PCR.

Strain construction

To visualize nuclear pore localization of the different domains of Nup131 and Nup132, *lys1*$^{+}$-integrating plasmids carrying GFPs65t-fused with respective Nup domains were introduced into cells with a *nup131*Δ*nup132*Δ double-mutant background. To construct the spNup96-spNup107 fusion Nup, a cDNA fragment encoding spNup107 or spNup107-GFP followed by a drug resistance marker gene was integrated after the chromosomal spNup96 coding region. After a diploid strain was obtained by crossing the yielded and wild type strains, the *nup107*$^{+}$ gene on the original chromosomal locus was deleted. To introduce the chromosomal fluorescent tag and gene disruption, a two-step PCR method was applied (Bähler et al, 1998). Nup-GFP fusion constructs were described previously (Asakawa et al., 2014). The spMis6-GFP fusion was constructed as described previously (Chikashige et al., 2004) or using the two-step PCR method. mCherry-spAtb2 was visualized as described previously (Yang et al., 2015).

Plasmid construction

To express the full-length or domains of the spNup131 and spNup132 proteins, cDNA fragments were amplified by PCR. The PCR products were sub-cloned into the *Bgl*II site of the plasmid of pY53 that carries the *nup132* promoter (-1000bp)-driven GFPs65t using the In-Fusion PCR cloning kit (Clontech Laboratories, Mountain View, CA, USA).

503 ***Preparation of whole cell extracts***

504 Growing cells (about 5×10^9) were collected and washed with 10 mM HEPES buffer
505 (pH 7.5) containing 1 mM PMSF. The washed cell pellet was suspended in 10 mM
506 HEPES buffer (pH 7.5) containing 1 mM PMSF, divided into aliquots of 3×10^8 cells,
507 and kept frozen by liquid nitrogen until use. To make a cell extract, the cell pellet was
508 thawed and suspended in 100 μL of lysis buffer (50 mM HEPES (pH 7.5), 150 mM
509 NaCl, 1% Triton X-100, 1 mM EDTA, 2 mM PMSF) with a protease inhibitor cocktail
510 (167-26081, Wako, Tokyo, Japan) and mashed by glass beads using Multi-beads
511 shocker (Yasui Kikai Corporation, Osaka, Japan). To prepare a whole cell extract from
512 spNup98-GFP expressing cells, the other lysis buffer (50mM HEPES pH7.5, 150mM
513 NaCl, 1mM EDTA, 2mM PMSF, 1% Triton, 0.1% SDS, 0.5% sodium deoxycholate)
514 with a protease inhibitor cocktail was used. After the further addition of 400 μL of lysis
515 buffer, the mashed cell pellet was transferred to new microtubes. The supernatant was
516 collected after centrifugation at 15 000 rpm for 15 min at 4°C and used as the
517 whole-cell extract.
518
519 ***Affinity-capture and LC/MS/MS analysis***
520 The whole-cell extract was incubated with a rabbit anti-GFP antibody (Rockland).
521 Antibody-conjugated proteins were collected by incubating with Protein A Sepharose
522 beads (17528001, GE Healthcare). Beads were then washed 4-5 times with the lysis
523 buffer described above. After elution in SDS-PAGE sample buffer, protein samples were
524 loaded onto a 12% SDS-PAGE gel for liquid chromatography coupled to tandem MS
525 (LC/MS/MS). Data analysis for LC/MS/MS was performed as described previously
526 (Nozawa et al., 2013) using the Pombase protein dataset released on November 12,

2015. The number of unique spectra and emPAI values (Ishihama et al., 2005) were computed from one measurement of all pieces of the gel. For spNup131 and spNup132, protein samples were prepared from two independent experiments and each preparation was analyzed by LC/MS/MS, and unique spectra detected for at least one of the samples were identified as interacting proteins with spNup131 and spNup132. For each of other Nups, protein samples from a single preparation were analyzed by LC/MS/MS.

Fluorescence microscopy

Images were obtained using a DeltaVision microscope system (GE Healthcare, Tokyo, Japan) equipped with a CoolSNAP HQ^2 CCD camera (Photometrics, Tucson, AZ, USA) through an oil-immersion objective lens (PlanApoN60×OSC; NA, 1.4) (Olympus, Tokyo, Japan) as described previously (Asakawa et al., 2014). Z-stack images were obtained and subjected to deconvolution that remove out-of-focus images to improve images as described previously. For time lapse microscopy, cells were observed every 5 minutes as described previously (Yang et al., 2015). The projection images of z-stacks were made by softWoRx software equipped in the microscope system.

Yeast two-hybrid assay

The yeast two-hybrid assay was performed according to the manufacturer's protocol (Clontech Laboratories). *S. pombe* Nup cDNAs were cloned into the pGAD424, pGBT9, and pBridge vectors. AH109 was used as the host strain. Spot assay was performed twice or three times for each test, and representative results were shown in Figure 4.

Acknowledgements

We thank the National BioResource Project Japan for the Nup cDNA clones. We also thank Drs. Thomas U. Schwartz and Valérie Doye for critical reading of this paper. This work was supported by the Uehara Memorial Foundation to TH and by the following JSPS KAKENHI grants: JP26440098 to HA; JP15K07066 to MI; JP15K06942 and JP15H01462 to KN; JP16H04739 and JP 25116004 to COb; JP26251037 and JP16H01309 to YH; JP25116006, JP26291007, and JP17K19505 to TH.

Competing financial interests

The authors declare no competing financial interests.

References

Alber F, Dokudovskaya S, Veenhoff LM, Zhang W, Kipper J, Devos D, Suprapto A, Schmidt OK, Williams R, Chait BT, Sali A. Rout MP. 2007. The molecular architecture of the nuclear pore complex. Nature 450: 695-701. doi:10.1038/nature06405

Amlacher S, Sarges P, Flemming D, van Noort V, Kunze R, Devos DP, Arumugam M, Bork P, Hurt E. 2011. Insight into structure and assembly of the nuclear pore complex by utilizing the genome of a eukaryotic thermophile. Cell 146: 277-286. doi:10.1016/j.cell.2011.06.039.

Asakawa H, Yang HJ, Yamamoto TG, Ohtsuki C, Chikashige Y, Sakata-Sogawa K, Tokunaga M, Iwamoto M, Hiraoka Y, Haraguchi T. 2014.Characterization of nuclear pore complex components in fission yeast *Schizosaccharomyces pombe*. Nucleus. 5: 149-162. doi:10.4161/nucl.28487

Asakawa H, Mori C, Ohtsuki C, Iwamoto M, Hiraoka Y, Haraguchi T. 2015.

575 Uncleavable Nup98-Nup96 is functional in the fission yeast *Schizosaccharomyces*
576 *pombe*. FEBS Open Bio. 5: 508-514. doi:10.1016/j.fob.2015.06.004.
577 Bähler J, Wu JQ, Longtine MS, Shah NG, McKenzie A 3rd, Steever AB, Wach A,
578 Philippsen P, Pringle JR. 1998. Heterologous modules for efficient and versatile
579 PCR-based gene targeting in *Schizosaccharomyces pombe*. Yeast. 14: 943-951.
580 doi:10.1002/(SICI)1097-0061(199807)14:10<943::AID-YEA292>3.0.CO;2-Y
581 Baï SW, Rouquette J, Umeda M, Faigle W, Loew D, Sazer S, Doye V. 2004. The fission
582 yeast Nup107-120 complex functionally interacts with the small GTPase Ran/Spi1
583 and is required for mRNA export, nuclear pore distribution, and proper cell division.
584 Mol Cell Biol. 24: 6379-6392. doi:10.1128/MCB.24.14.6379-6392.2004
585 Belgareh N, Rabut G, Baï SW, van Overbeek M, Beaudouin J, Daigle N, Zatsepina OV,
586 Pasteau F, Labas V, Fromont-Racine M, Ellenberg J, Doye V. 2001. An
587 evolutionarily conserved NPC subcomplex, which redistributes in part to
588 kinetochores in mammalian cells. J Cell Biol. 154: 1147-1160.
589 doi:10.1083/jcb.200101081
590 Bilokapic S, Schwartz TU. 2012. Molecular basis for Nup37 and ELY5/ELYS
591 recruitment to the nuclear pore complex. Proc Natl Acad Sci U S A. 109:
592 15241-15246. doi:10.1073/pnas.1205151109
593 Boehmer T, Enninga J, Dales S, Blobel G, Zhong H. 2003. Depletion of a single
594 nucleoporin, Nup107, prevents the assembly of a subset of nucleoporins into the
595 nuclear pore complex. Proc Natl Acad Sci U S A. 100: 981-985.
596 doi:10.1073/pnas.252749899
597 Bui KH, von Appen A, DiGuilio AL, Ori A, Sparks L, Mackmull MT, Bock T, Hagen W,
598 Andrés-Pons A, Glavy JS, Beck M. 2013. Integrated structural analysis of the

599 human nuclear pore complex scaffold. Cell. 155: 1233-1243.
600 doi:10.1016/j.cell.2013.10.055
601 Chen XQ, Du X, Liu J, Balasubramanian MK, Balasundaram D. 2004. Identification of
602 genes encoding putative nucleoporins and transport factors in the fission yeast
603 *Schizosaccharomyces pombe*: a deletion analysis. Yeast. 21: 495-509.
604 doi:10.1002/yea.1115
605 Chikashige Y, Kurokawa R, Haraguchi T, Hiraoka Y. 2004. Meiosis induced by
606 inactivation of Pat1 kinase proceeds with aberrant nuclear positioning of
607 centromeres in the fission yeast *Schizosaccharomyces pomb*e. Genes Cells. 9:
608 671-684. doi:10.1111/j.1356-9597.2004.00760.x
609 Cho AR, Yang KJ, Bae Y, Bahk YY, Kim E, Lee H, Kim JK, Park W, Rhim H, Choi SY,
610 Imanaka T, Moon S, Yoon J, Yoon SK. 2009. Tissue-specific expression and
611 subcellular localization of ALADIN, the absence of which causes human triple A
612 syndrome. Exp. Mol. Med. 41: 381–386. doi:10.3858/emm.2009.41.6.043
613 Cronshaw JM, Krutchinsky AN, Zhang W, Chait BT, Matunis MJ. 2002. Proteomic
614 analysis of the mammalian nuclear pore complex. J Cell Biol. 158: 915-927.
615 doi:10.1083/jcb.200206106
616 D'Angelo MA, Anderson DJ, Richard E, Hetzer MW. 2006. Nuclear pores form de novo
617 from both sides of the nuclear envelope. Science. 312: 440-443.
618 doi:10.1126/science.1124196
619 D'Angelo MA, Raices M, Panowski SH, Hetzer MW. 2009. Age-dependent
620 deterioration of nuclear pore complexes causes a loss of nuclear integrity in
621 postmitotic cells. Cell 136: 284-295. doi:10.1016/j.cell.2008.11.037
622 D'Angelo MA, Gomez-Cavazos JS, Mei A, Lackner DH, Hetzer MW. 2012. A change in

623 nuclear pore complex composition regulates cell differentiation. Dev Cell. 22:
624 446-458. doi: 10.1016/j.devcel.2011.11.021
625 DeGrasse JA, DuBois KN, Devos D, Siegel TN, Sali A, Field MC, Rout MP, Chait BT.
626 2009. Evidence for a shared nuclear pore complex architecture that is conserved
627 from the last common eukaryotic ancestor. Mol Cell Proteomics. 8: 2119-2130.
628 doi:10.1074/mcp.M900038-MCP200
629 Fernandez-Martinez J, Phillips J, Sekedat MD, Diaz-Avalos R, Velazquez-Muriel J,
630 Franke JD, Williams R, Stokes DL, Chait BT, Sali A, Rout MP. 2012.
631 Structure-function mapping of a heptameric module in the nuclear pore complex. J.
632 Cell Biol. 196: 419-434. doi:10.1083/jcb.201109008
633 Fischer J, Teimer R, Amlacher S, Kunze R, Hurt E. 2015. Linker Nups connect the
634 nuclear pore complex inner ring with the outer ring and transport channel. Nat
635 Struct Mol Biol. 22: 774-781. doi:10.1038/nsmb.3084
636 Flemming D, Thierbach K, Stelter P, Böttcher B, Hurt E. 2010. Precise mapping of
637 subunits in multiprotein complexes by a versatile electron microscopy label. Nat
638 Struct Mol Biol. 17: 775-778. doi:10.1038/nsmb.1811
639 Frost A, Elgort MG, Brandman O, Ives C, Collins SR, Miller-Vedam L, Weibezahn J,
640 Hein MY, Poser I, Mann M, Hyman AA, Weissman JS. 2012. Functional
641 repurposing revealed by comparing *S. pombe* and *S. cerevisiae* genetic interactions.
642 Cell. 149: 1339-1352. doi:10.1016/j.cell.2012.04.028
643 Goudreault M, D'Ambrosio LM, Kean MJ, Mullin MJ, Larsen BG, Sanchez A,
644 Chaudhry S, Chen GI, Sicheri F, Nesvizhskii AI, Aebersold R, Raught B, Gingras
645 AC. 2009. A PP2A phosphatase high density interaction network identifies a novel
646 striatin-interacting phosphatase and kinase complex linked to the cerebral

cavernous malformation 3 (CCM3) protein. Molecular & Cellular Proteomics. 8:157-171. doi:10.1074/mcp.M800266-MCP200

Griffis ER, Xu S, Powers MA. 2003. Nup98 localizes to both nuclear and cytoplasmic sides of the nuclear pore and binds to two distinct nucleoporin subcomplexes. Mol Biol Cell. 14: 600-610. doi:10.1091/mbc.E02-09-0582

Guindon, S., Dufayard, J.F., Lefort, V., Anisimova, M., Hordijk, W. & Gascuel, O. New algorithms and methods to estimate maximum-likelihood phylogenies: assessing the performance of PhyML 3.0. Syst Biol. 59, 307-321 (2010). doi: 10.1093/sysbio/syq010

Harel A, Orjalo AV, Vincent T, Lachish-Zalait A, Vasu S, Shah S, Zimmerman E, Elbaum M, Forbes DJ. 2003. Removal of a single pore subcomplex results in vertebrate nuclei devoid of nuclear pores. Mol Cell. 11: 853-864. doi:10.1016/S1097-2765(03)00116-3

Hodel AE, Hodel MR, Griffis ER, Hennig KA, Ratner GA, Xu S, Powers MA. 2002. The three-dimensional structure of the autoproteolytic, nuclear pore-targeting domain of the human nucleoporin Nup98. Mol Cell. 10: 347-358. doi:10.1016/S1097-2765(02)00589-0

Huerta-Cepas, J., Serra, F. & Bork, P. ETE 3: Reconstruction, Analysis, and Visualization of Phylogenomic Data. Mol Biol Evol. 33, 1635-1638 (2016). doi:10.1093/molbev/msw046

Ishihama Y, Oda Y, Tabata T, Sato T, Nagasu T, Rappsilber J, Mann M. 2005. Exponentially modified protein abundance index (emPAI) for estimation of absolute protein amount in proteomics by the number of sequenced peptides per protein. Mol Cell Proteomics. 4: 1265-1272. doi:10.1074/mcp.M500061-MCP200

671 Iwamoto M, Asakawa H, Ohtsuki C, Osakada H, Koujin T, Hiraoka Y, Haraguchi T.
672 2013. Monoclonal antibodies recognize Gly-Leu-Phe-Gly repeat of nucleoporin
673 Nup98 of *Tetrahymena*, yeasts, and humans. Monoclon Antib Immunodiagn
674 Immunother. 32: 81-90. doi: 10.1089/mab.2012.0118
675 Iwamoto M, Osakada H, Mori C, Fukuda Y, Nagao K, Obuse C, Hiraoka Y, Haraguchi T.
676 2017. Compositionally distinct nuclear pore complexes of functionally distinct
677 dimorphic nuclei in the ciliate *Tetrahymena*. J Cell Sci. 130: 1822-1834.
678 doi:10.1242/jcs.199398
679 Kampmann M, Blobel G. 2009. Three-dimensional structure and flexibility of a
680 membrane-coating module of the nuclear pore complex. Nat Struct Mol Biol. 16:
681 782-788. doi:10.1038/nsmb.1618
682 Karrer KM. 2012. Nuclear dualism. Methods Cell Biol. 109: 29-52.
683 doi:10.1016/B978-0-12-385967-9.00003-7
684 Kelley K, Knockenhauer KE, Kabachinski G, Schwartz TU. 2015. Atomic structure of
685 the Y complex of the nuclear pore. Nat Struct Mol Biol. 22: 425-431.
686 doi:10.1038/nsmb.2998
687 Knockenhauer KE, Schwartz TU. 2016. The nuclear pore complex as a flexible and
688 dynamic gate. Cell. 164: 1162-1171. doi:10.1016/j.cell.2016.01.034
689 Kosinski J, Mosalaganti S, von Appen A, Teimer R, DiGuilio AL, Wan W, Bui KH,
690 Hagen WJ, Briggs JA, Glavy JS, Hurt E, Beck M. 2016. Molecular architecture of
691 the inner ring scaffold of the human nuclear pore complex. Science. 352: 363-365.
692 doi: 10.1126/science.aaf0643
693 Lin DH, Stuwe T, Schilbach S, Rundlet EJ, Perriches T, Mobbs G, Fan Y, Thierbach K,
694 Huber FM, Collins LN, Davenport AM, Jeon YE, Hoelz A. 2016. Architecture of

the symmetric core of the nuclear pore. Science. 352, aaf1015. doi:10.1126/science.aaf1015

Liu HL, De Souza CP, Osmani AH, Osmani SA. 2009. The three fungal transmembrane nuclear pore complex proteins of *Aspergillus nidulans* are dispensable in the presence of an intact An-Nup84-120 complex. Mol. Biol. Cell. 20: 616-630. doi:10.1091/mbc.E08-06-0628.

Liu NN, Han TX, Du LL, Zhou JQ. 2010. A genome-wide screen for *Schizosaccharomyces pombe* deletion mutants that affect telomere length. Cell Res. 20: 963-965. doi:10.1038/cr.2010.107

Loïodice I, Alves A, Rabut G, Van Overbeek M, Ellenberg J, Sibarita JB, Doye V. 2004. The entire Nup107-160 complex, including three new members, is targeted as one entity to kinetochores in mitosis. Mol Biol Cell. 15: 3333-3344. doi:10.1091/mbc.E03-12-0878

Lutzmann M, Kunze R, Buerer A, Aebi U, Hurt E. 2002. Modular self-assembly of a Y-shaped multiprotein complex from seven nucleoporins. EMBO J. 21: 387-397. doi:10.1093/emboj/21.3.387

Mishra RK, Chakraborty P, Arnaoutov A, Fontoura BM, Dasso M. 2010. The Nup107-160 complex and gamma-TuRC regulate microtubule polymerization at kinetochores. Nat Cell Biol. 12: 164-169. doi:10.1038/ncb2016

Moreno CS, Lane WS, Pallas DC. 2001. A mammalian homolog of yeast MOB1 is both a member and a putative substrate of striatin family-protein phosphatase 2A complexes. J. Biol. Chem. 276: 24253–24260. doi:10.1074/jbc.M102398200

Moreno S, Klar A, Nurse P. 1991. Molecular genetic analysis of fission yeast *Schizosaccharomyces pombe*. Methods Enzymol. 194: 795-823.

719 doi:10.1016/0076-6879(91)94059-L

720 Nozawa RS, Nagao K, Igami KT, Shibata S, Shirai N, Nozaki N, Sado T, Kimura H,
721 Obuse C. 2013. Human inactive X chromosome is compacted through a
722 polycomb-independent SMCHD1-HBiX1 pathway. Nature Structure & Molecular
723 Biology 20: 566–573. doi:10.1038/nsmb.2532

724 Nie M, Boddy MN. 2015. Pli1(PIAS1) SUMO ligase protected by the nuclear
725 pore-associated SUMO protease Ulp1SENP1/2. J Biol Chem. 290: 22678-22685.
726 doi:10.1074/jbc.M115.673038

727 Obado SO, Brillantes M, Uryu K, Zhang W, Ketaren NE, Chait BT, Field MC, Rout MP.
728 2016. Interactome mapping teveals the evolutionary history of the nuclear pore
729 complex. PLoS Biol. 14: e1002365. doi:10.1371/journal.pbio.1002365

730 Olsson M, Schéele S, Ekblom P. 2004. Limited expression of nuclear pore membrane
731 glycoprotein 210 in cell lines and tissues suggests cell-type specific nuclear pores in
732 metazoans. Exp Cell Res. 292, 359-370. doi:10.1016/j.yexcr.2003.09.014

733 Ori A, Banterle N, Iskar M, Andrés-Pons A, Escher C, Bui KH, Sparks L,
734 Solis-Mezarino V, Rinner O, Bork P, Lemke EA, Beck M. 2013. Cell type-specific
735 nuclear pores: a case in point for context-dependent stoichiometry of molecular
736 machines. Mol Syst Biol. 9: 648. doi:10.1038/msb.2013.4.

737 Orjalo AV, Arnaoutov A, Shen Z, Boyarchuk Y, Zeitlin SG, Fontoura B, Briggs S, Dasso
738 M, Forbes DJ. 2006. The Nup107-160 nucleoporin complex is required for correct
739 bipolar spindle assembly. Mol Biol Cell. 17: 3806-3818.
740 doi:10.1091/mbc.E05-11-1061

741 Platani M, Santarella-Mellwig R, Posch M, Walczak R, Swedlow JR, Mattaj IW. 2009.
742 The Nup107-160 nucleoporin complex promotes mitotic events via control of the

743 localization state of the chromosome passenger complex. Mol Biol Cell. 20:
744 5260-5275. doi:10.1091/mbc.E09-05-0377
745 Rasala BA, Orjalo AV, Shen Z, Briggs S, Forbes DJ. 2006. ELYS is a dual
746 nucleoporin/kinetochore protein required for nuclear pore assembly and proper cell
747 division. Proc Natl Acad Sci U S A. 103: 17801-17806.
748 doi:10.1073/pnas.0608484103
749 Raices M, D'Angelo MA. 2012. Nuclear pore complex composition: a new regulator of
750 tissue-specific and developmental functions. Nat Rev Mol Cell Biol. 13: 687-699.
751 doi:10.1038/nrm3461
752 Ratner GA, Hodel AE, Powers MA.2007. Molecular determinants of binding between
753 Gly-Leu-Phe-Gly nucleoporins and the nuclear pore complex. J Biol Chem. 282:
754 33968-33976. doi:10.1074/jbc.M707911200
755 Rout MP, Aitchison JD, Suprapto A, Hjertaas K, Zhao Y, Chait BT. 2000. The yeast
756 nuclear pore complex: composition, architecture, and transport mechanism. J Cell
757 Biol. 148: 635-651. doi:10.1083/jcb.148.4.635
758 Saitoh S, Takahashi K, Yanagida M. 1997. Mis6, a fission yeast inner centromere
759 protein, acts during G1/S and forms specialized chromatin required for equal
760 segregation. Cell. 90: 131-143. doi:10.1016/S0092-8674(00)80320-7
761 Sievers, F. & Higgins, D.G. Clustal Omega, accurate alignment of very large numbers
762 of sequences. Methods Mol Biol. 1079, 105-116 (2014). doi:
763 10.1007/978-1-62703-646-7_6
764 Singh NS, Shao N, McLean JR, Sevugan M, Ren L, Chew TG, Bimbo A, Sharma R,
765 Tang X, Gould KL, Balasubramanian MK. 2011. SIN-inhibitory phosphatase
766 complex promotes Cdc11p dephosphorylation and propagates SIN asymmetry in

767 fission yeast. Curr Biol. 21: 1968-1978. doi:10.1016/j.cub.2011.10.051
768 Stuwe T, von Borzyskowski LS, Davenport AM, Hoelz A. 2012. Molecular basis for the
769 anchoring of proto-oncoprotein Nup98 to the cytoplasmic face of the nuclear pore
770 complex. J Mol Biol. 419: 330-346. doi:10.1016/j.jmb.2012.03.024
771 Stuwe T, Correia AR, Lin DH, Paduch M, Lu VT, Kossiakoff AA, Hoelz A. 2015.
772 Nuclear pores. Architecture of the nuclear pore complex coat. Science. 347:
773 1148-1152. doi:10.1126/science.aaa4136
774 Stuwe T, Bley CJ, Thierbach K, Petrovic S, Schilbach S, Mayo DJ, Perriches T, Rundlet
775 EJ, Jeon YE, Collins LN, Huber FM, Lin DH, Paduch M, Koide A, Lu V, Fischer J,
776 Hurt E, Koide S, Kossiakoff AA, Hoelz A. 2015. Architecture of the fungal nuclear
777 pore inner ring complex. Science. 350: 56-64. doi:10.1126/science.aac9176
778 Tamura K, Fukao Y, Iwamoto M, Haraguchi T, Hara-Nishimura I. 2010. Identification
779 and characterization of nuclear pore complex components in *Arabidopsis thaliana*.
780 Plant Cell. 22: 4084-4097. doi:10.1105/tpc.110.079947
781 Thierbach K, von Appen A, Thoms M, Beck M, Flemming D, Hurt E. 2013. Protein
782 interfaces of the conserved Nup84 complex from *Chaetomium thermophilum*
783 shown by crosslinking mass spectrometry and electron microscopy. Structure. 21:
784 1672-1682. doi:10.1016/j.str.2013.07.004
785 von Appen A, Kosinski J, Sparks L, Ori A, DiGuilio AL, Vollmer B, Mackmull MT,
786 Banterle N, Parca L, Kastritis P, Buczak K, Mosalaganti S, Hagen W, Andres-Pons
787 A, Lemke EA, Bork P, Antonin W, Glavy JS, Bui KH, Beck M. 2015. *In situ*
788 structural analysis of the human nuclear pore complex. Nature. 526: 140-143.
789 doi:10.1038/nature15381
790 Walther TC, Alves A, Pickersgill H, Loïodice I, Hetzer M, Galy V, Hülsmann BB,

791 Köcher T, Wilm M, Allen T, Mattaj IW, Doye V. 2003. The conserved Nup107-160
792 complex is critical for nuclear pore complex assembly. Cell. 113: 195-206.
793 doi:10.1016/S0092-8674(03)00235-6
794 Whittle JR, Schwartz TU. 2009. Architectural nucleoporins Nup157/170 and Nup133
795 are structurally related and descend from a second ancestral element. J Biol Chem.
796 284: 28442-28452. doi:10.1074/jbc.M109.023580
797 Yang HJ, Asakawa H, Haraguchi T, Hiraoka Y. 2015. Nup132 modulates meiotic
798 spindle attachment in fission yeast by regulating kinetochore assembly. J Cell Biol.
799 211: 295-308. doi:10.1083/jcb.201501035
800 Zuccolo M, Alves A, Galy V, Bolhy S, Formstecher E, Racine V, Sibarita JB, Fukagawa
801 T, Shiekhattar R, Yen T, Doye V. 2007. The human Nup107-160 nuclear pore
802 subcomplex contributes to proper kinetochore functions. EMBO J. 26: 1853-1864.
803 doi:10.1038/sj.emboj.7601642
804

Figure legends

Figure 1. Localization of spNup131 and spNup132 at NPCs. **(a)** Distribution of secondary structure elements on spNup131 and spNup132. Both spNup131 and spNup132 have structural features in common with Nup133 found in many organisms, such as the N-terminal β-propeller rich region assigned as the Nup133 N-terminal like domain (Pfam PF08801; amino acid residues 44–454 in spNup131 and 50–440 in spNup132) and the C-terminal α-helical stack region assigned as the Non-repetitive/WGA-negative nucleoporin C-terminal domain (Pfam PF03177; a.a. residues 581–1049 in spNup131 and 515–1084 in spNup132). **(b)** IEM of GFP-spNup131 and GFP-spNup132. Arrows indicate the nuclear pores. Scale bar, 100 nm. **(c)** Quantitative representation of IEM for N-terminally tagged spNup131 and spNup132. (left) A montage image of 20 immunoelectron micrographs. The diameter of the circle is 200 nm. (right) A schematic drawing illustrating the distribution of immunogold particles shown in the montage image. Red dots represent the pore centers. **(d)** Quantitative representation of IEM for C-terminally tagged spNup131 and spNup132. Montage pictures and distributions of immunogold particles are shown as described in **(c)**.

Figure 1–figure supplement 1. Phylogenetic tree of Nup133-like proteins. Species names and Genbank accession numbers are shown. spNup131- and spNup132-like proteins found in fission yeasts are colored. Alignment and phylogenetic reconstructions were performed using the “build” function of ETE3 v3.0.0b32 (Huerta-Cepas et al., 2016) implemented on GenomeNet (http://www.genome.jp/tools/ete/). Alignment was performed using Clustal Omega

v1.2.1 with default options (Sievers and Higgins, 2014). The ML tree was inferred using PhyML v20160115 run with model JTT (Guindon et al., 2010). Branch supports are the Chi^2-based parametric values determined using the approximate likelihood ratio test.

Figure 1–figure supplement 2. IEM of spMis6, spNup131 and spNup132.

(a) IEM of spMis6-GFP. An original electron micrograph (left) and its duplicated image (right) indicating subcellular structures are shown. SPB, spindle pole body; NE, nuclear envelope. **(b)** IEM of coexpressed GFP-spNup131 and spMis6-GFP. A representative image is shown. Arrows indicate immunogold at the nuclear pores. The yellow-lined regions indicate immunogold near the SPB, corresponding to the signals from spMis6-GFP. **(c, d)** Immunoelectron micrographs of 20 nuclear pores used to generate the montage picture and distribution analysis in **Fig. 1(c)**. Scale bars, 200 nm. **(c)** IEM of GFP-spNup131 and spMis6-GFP. **(d)** IEM of GFP-spNup132.

Figure 2. IEM of *S. pombe* Nups. Immunogold distribution of the projected immunoelectron micrographs is shown as a quantitative representation for each Nup (see Materials and Methods for details). **(a)** Nup107–160 subcomplex Nups. **(b)** Nup93 subcomplex Nups. **(c)** Channel Nups. IEM for spNup98 was performed using anti-GLFG repeats antibody for the wild type strain and anti-GFP antibody for the spNup98-GFP strain. **(d)** Nsp1. **(e)** Cytoplasmic Nups. **(f)** Nuclear basket Nups. **(g)** Transmembrane Nups.

Figure 2–figure supplement 1. Phylogenetic tree of Nup93-like proteins.

Species names and Genebank accession numbers are shown. spNpp106- and

853 spNup97-like proteins found in fission yeasts are colored. Amino acid sequences were
854 analyzed as described in **Figure 1–figure supplement 1**.
855
856 **Figure 3–figure supplement 1. Gels for MS analysis of immunoprecipitates with**
857 **GFP or GFP-tagged Nups.**
858 Images of Coomassie-stained SDS-PAGE gels are shown. Arrows indicate positions of
859 GFP-tagged proteins. Dots indicate the positions of molecular weight marker proteins
860 shown at the far left.
861
862 **Figure 3.** Heat map of semi-quantified abundance (emPAI) of nucleoporins. Nups on
863 the top row are nucleoporins detected by MS analysis of the sample precipitated with
864 each GFP-Nup as a bait. The color code was determined using emPAI values. White
865 boxes indicate no Nups detected. Blue boxes indicate subcomplexes with mutual
866 connections between components. Pink boxes indicate subcomplexes with connections
867 to other subcomplexes.
868
869 **Figure 4.** Interactions *S. pombe* Nup107-160 subcomplex Nups. **(a)** Yeast two-hybrid
870 assay of spNup131, spNup132, spNup107, spNup96, spNup85, and spNup120. AD,
871 transcriptional activation domain; BD, DNA-binding domain. BD-fused spNup120 and
872 BD-fused spNup85 were not used in this experiment because they themselves showed
873 transcriptional activation activity. **(b)** Yeast three-hybrid assay of spNup96, spNup85,
874 and spNup120. BD-spNup96 or BD alone was expressed with or without spNup85
875 expression from a BD vector. **(c)** Yeast two-hybrid assay of spEly5, spNup37, spSeh1
876 plus spNup85, and spNup120. **(d)** Yeast three-hybrid assay of spEly5, spNup37, and

877 spNup120. BD-spEly5 or BD alone was expressed with or without spNup37. **(e)** Yeast
878 two-hybrid assay of spEly5 and spNup37.
879
880 **Figure 5.** Model of the *S. pombe* NPC. Positions of each subcomplex were deduced
881 according to IEM and mass spectrometry results in this study. Solid line indicates the
882 direct interaction of Nups demonstrated by yeast two-hybrid assays. Broken line
883 indicates the interaction of Nups demonstrated by mass spectrometry.
884
885 **Figure 6.** Localization of the spNup131 and spNup132 domains. **(a)** Schematics of the
886 spNup131 and spNup132 fragments. **(b)** Localization of spNup131 and spNup132
887 fragments as determined by FM. GFP-fused fragments were expressed under the
888 spNup132 promoter in the background of the *nup131Δ nup132Δ* double mutant.
889 spCut11-mCherry served as an NPC marker. Scale bar, 5 μm. **(c)** IEM of the spNup131
890 and spNup132 fragments. Projection images (left) and immunogold distributions (right)
891 are shown as described in the legend of **Fig.1(c)**. The red points indicate the pore
892 centers. **(d)** Yeast two-hybrid assay. AD and BD indicate the transcriptional activation
893 domain and the DNA binding domain, respectively.
894
895 **Figure 7.** Localization and functional analysis of spNup96-spNup107 fusion Nup. **(a)**
896 Western Blot analysis of the spNup96-spNup107-GFP fusion protein. Asterisks
897 represent non-specific cross reactions of anti-GFP antibody. **(b)** IEM of the
898 spNup96-spNup107 fusion protein. Immunogold distribution of the projected
899 immunoelectron micrographs is shown. **(c)** IEM of GFP-spNup132 in the background
900 of spNup96-spNup107 fusion. **(d)** A cell growth assay in the presence (+TBZ) or

absence (-TBZ) of the microtubule-destabilizing drug TBZ. Five-fold serial dilutions of wild type and spNup96-spNup107 fusion strain were spotted on YES medium containing or lacking TBZ and incubated for 3 days. **(e)** Time-lapse observation of *S. pombe* cells (wt or spNup96-spNup107 fusion strain) undergoing meiosis. Cells expressing mCherry-fused α-tubulin (spAtb2) were induced to enter meiosis. The duration of meiosis I and II was determined as the time the spindle was present. Dotted lines show cell shapes. The time 0 indicates a time for the first appearance of meiosis I spindle formation. Representative images are shown (number of cells observed: 32 for wild type and 33 for spNup96-spNup107). **(f)** Statistical analysis for images obtained in **(e)**. Duration of meiosis I and II. Error bars represent standard deviations. The duration of meiosis I was 28.4 ± 3.0 min in wild type and 37.9 ± 6.3 min in spNup96-spNup107 fusion cells. The duration of meiosis II was 25.8 ± 1.8 min in wild type and 29.8 ± 2.9 min in spNup96-spNup107 fusion cells. Asterisks indicate statistical significance ($p < 0.0001$) between indicated strains as revealed by Welch's t-test. Number of cells observed: 32 for wild type and 33 for spNup96-spNup107. **(g)** Abnormal spore formation was observed in the background of spNup96-spNup107 fusion. More than 200 asci were counted for each strain.

Figure 8. spNup131 interacts with spFar8. **(a)** spFar8-GFP localizes at the nuclear periphery in an spNup131-dependent manner. Far8-GFP was expressed in the indicated strains, and cells exponentially growing in EMM2 liquid medium were observed by FM. spCut11-mCherry was observed as an NPC marker. Scale bar, 10 μm. **(b)** NPC-dependent localization of spFar8-GFP. Wild type and *nup132Δ* cells expressing spFar8-GFP were cultured on a YES agar plate at 30˚C for 3 days and observed by FM.

925 spCut11-mCherry was observed as an NPC marker. Scale bar, 10 μm. **(c)** Western blot
926 analysis of spFar8-GFP. Whole cell extracts were prepared from wild type, *nup131*Δ,
927 and *nup132*Δ cells expressing spFar8-GFP and subjected to SDS-PAGE and Western
928 blot analysis. spFar8-GFP was detected with anti-GFP antibody. spNup98 was detected
929 by the anti-Nup98 antibody 13C2 for a loading control. An arrow indicates the position
930 of spFar8-GFP. **(d)** spNup131-dependent localization of spFar11-GFP. Cells were
931 prepared and observed as described in **(a)**. Scale bar, 10 μm.

Asakawa et al. Figure 1

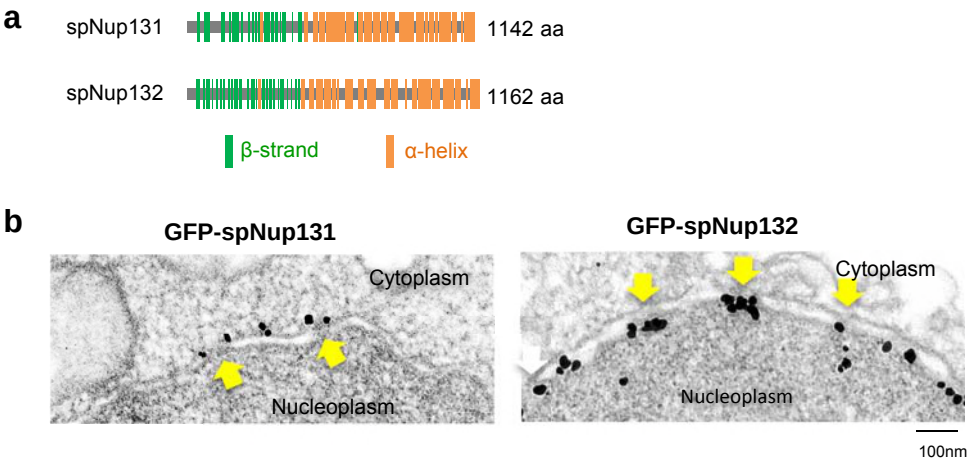

Asakawa et al. Figure 1–figure supplement 1

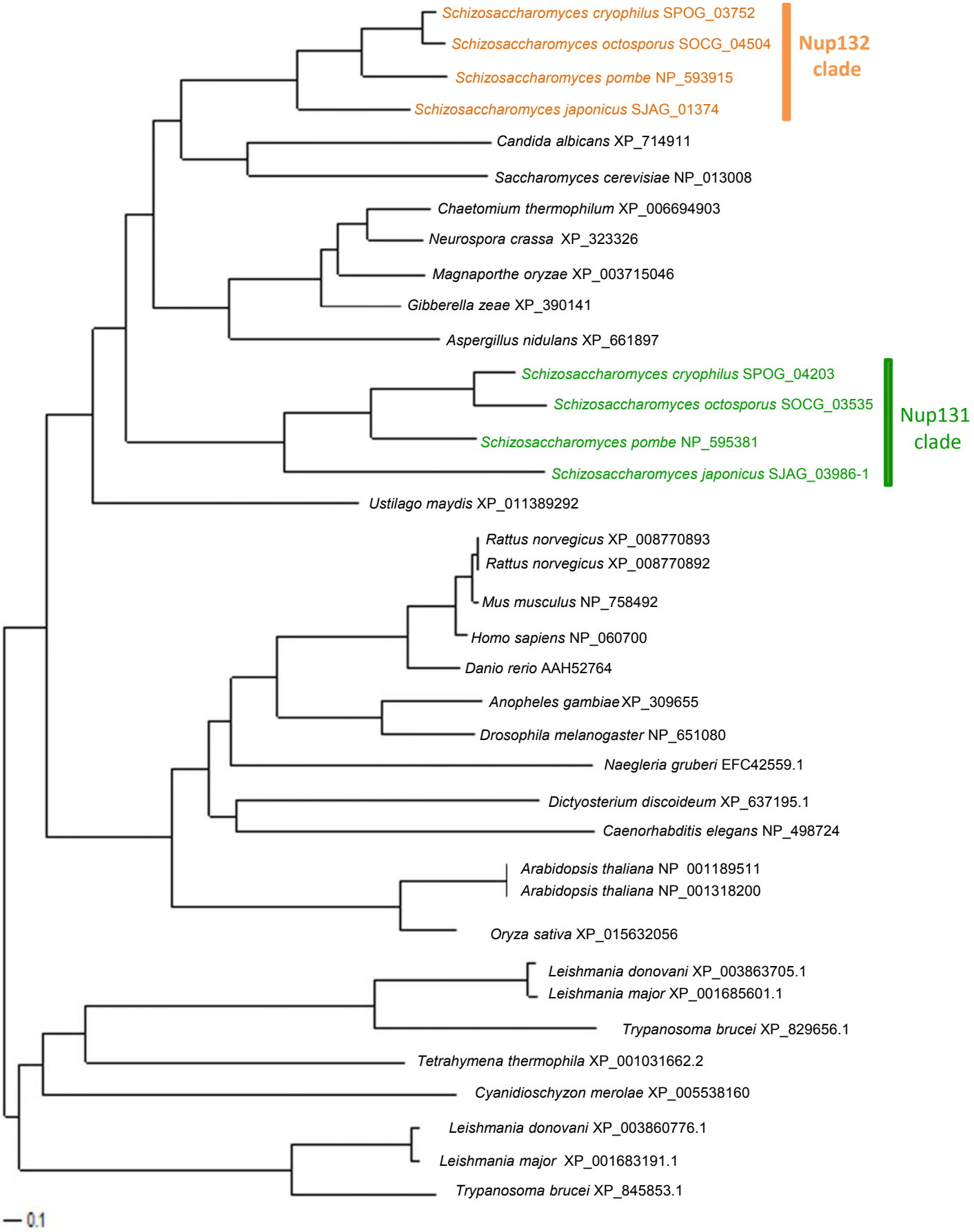

Asakawa et al. Figure 1–figure supplement 2

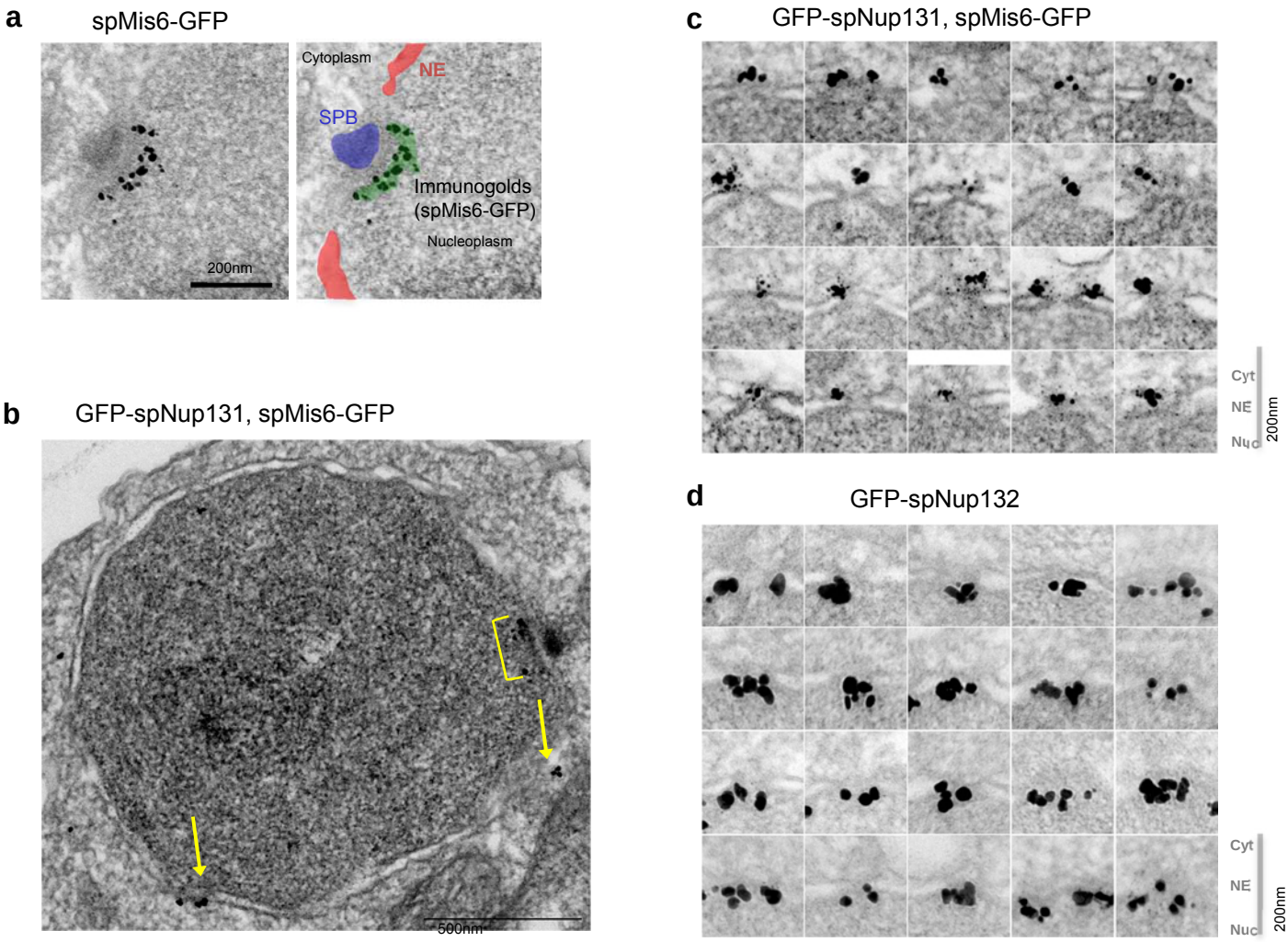

Asakawa et al. Figure 2

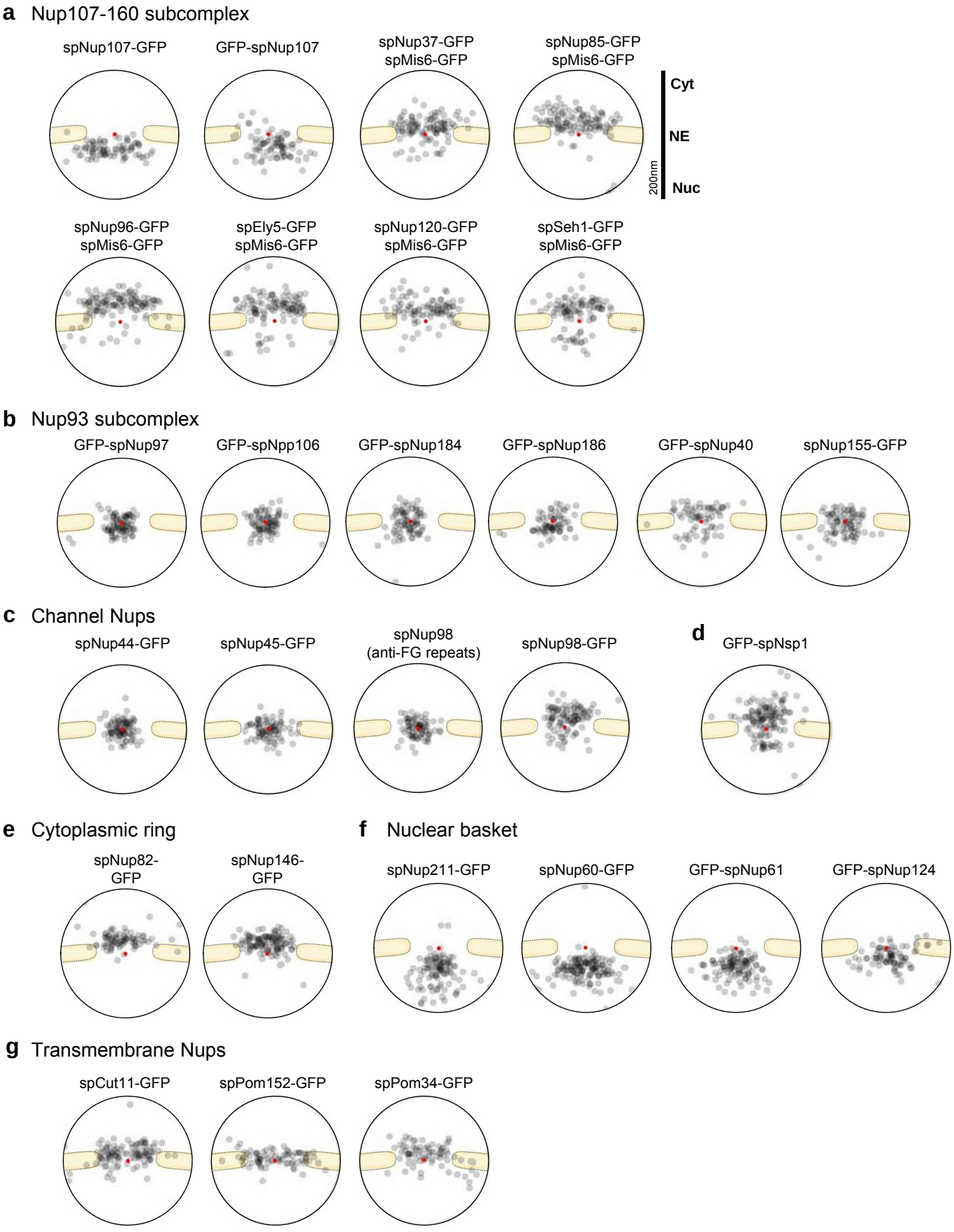

Asakawa et al. Figure 2–figure supplement 1

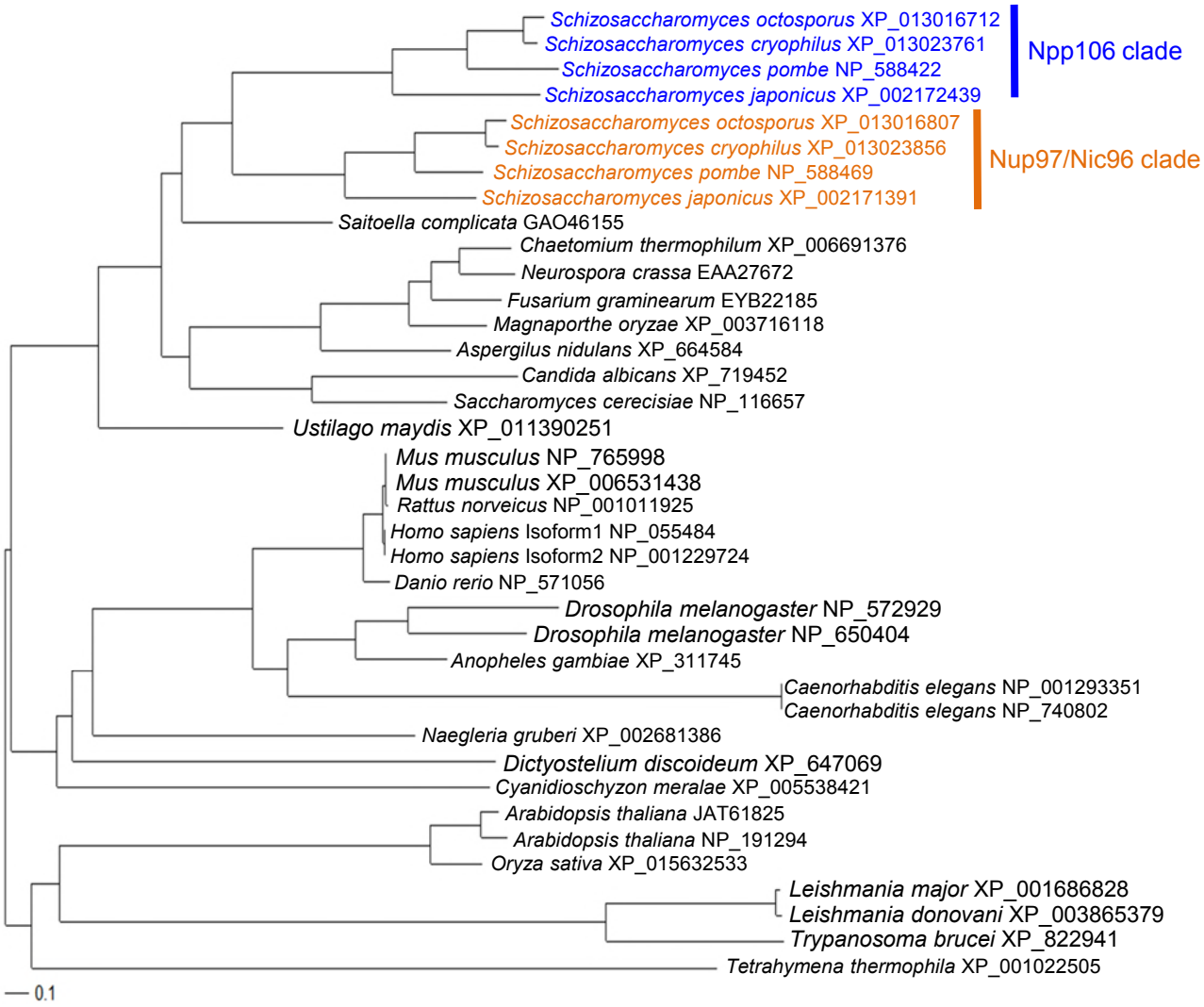

Asakawa et al. Figure 3

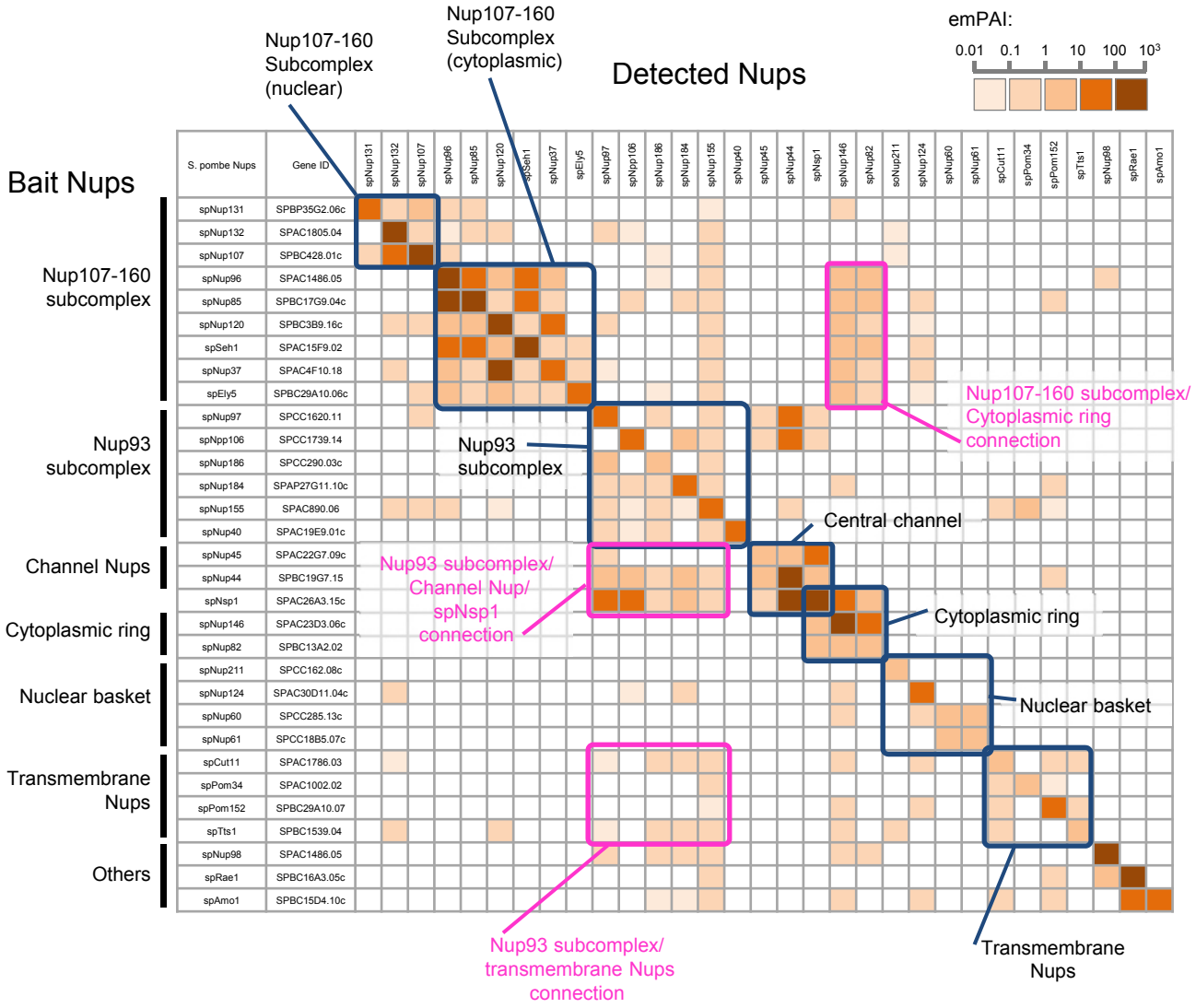

Asakawa et al. Figure 3–figure supplement 1

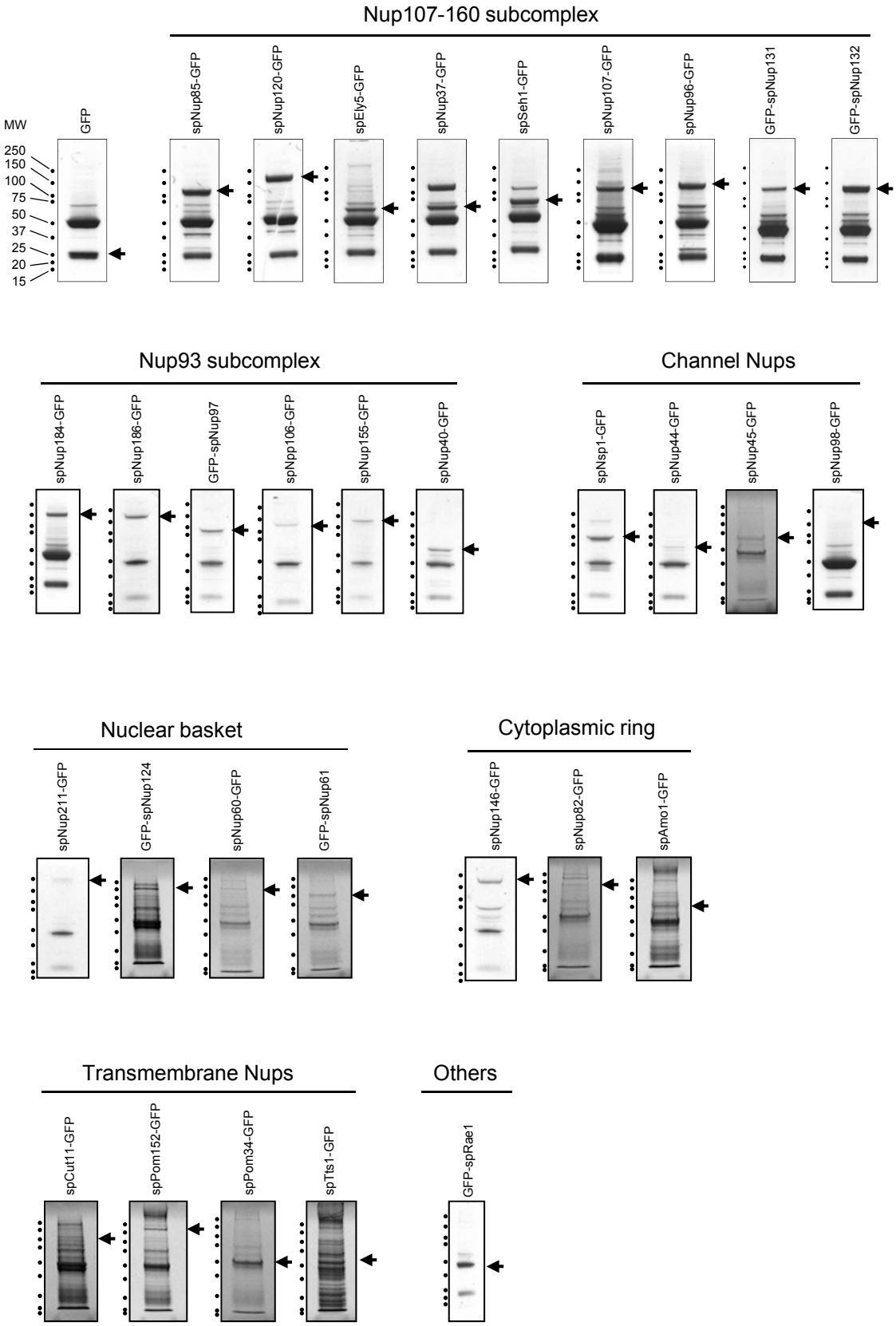

Asakawa et al. Figure 4

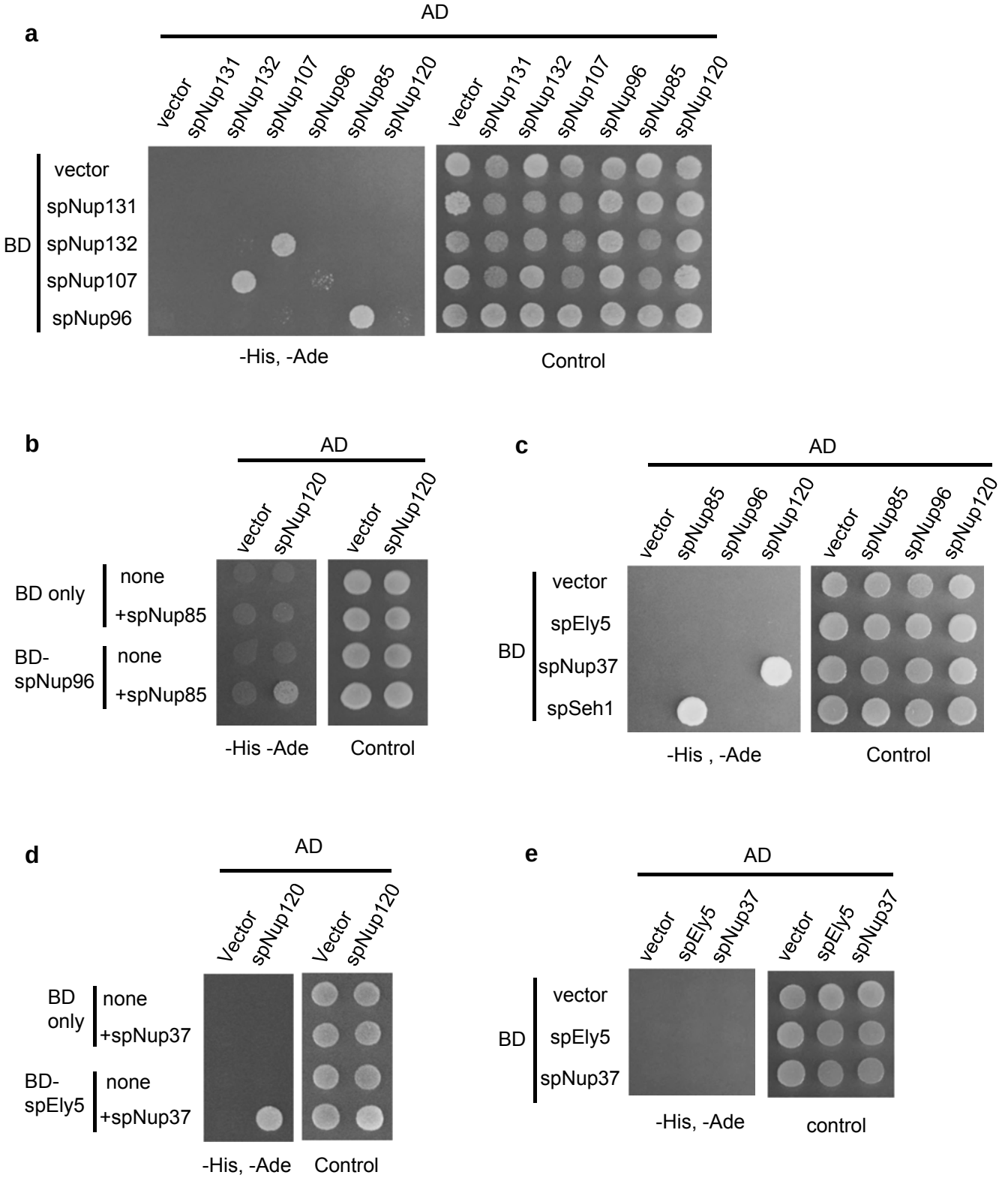

Asakawa et al. Figure 5

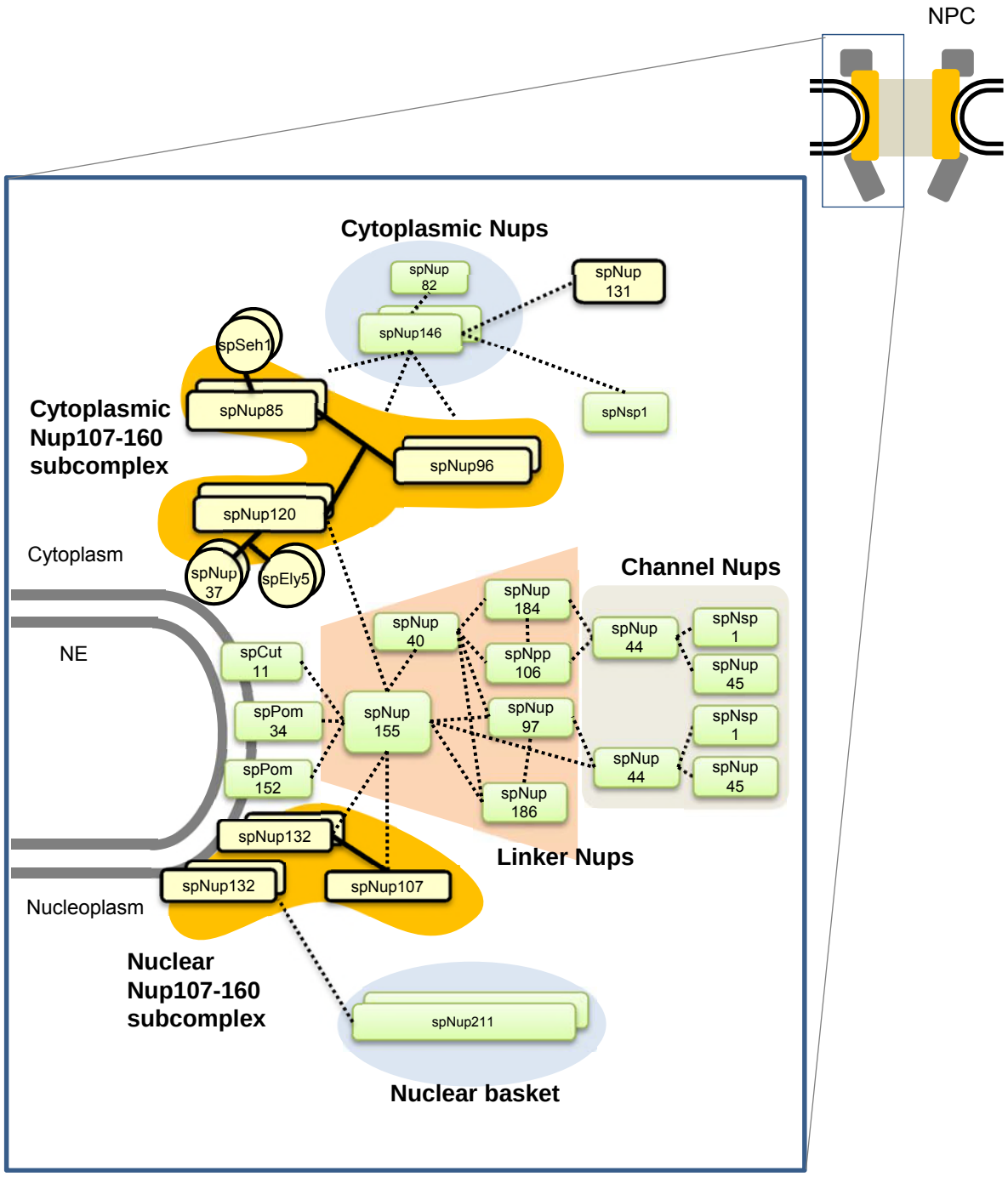

Asakawa et al. Figure 6

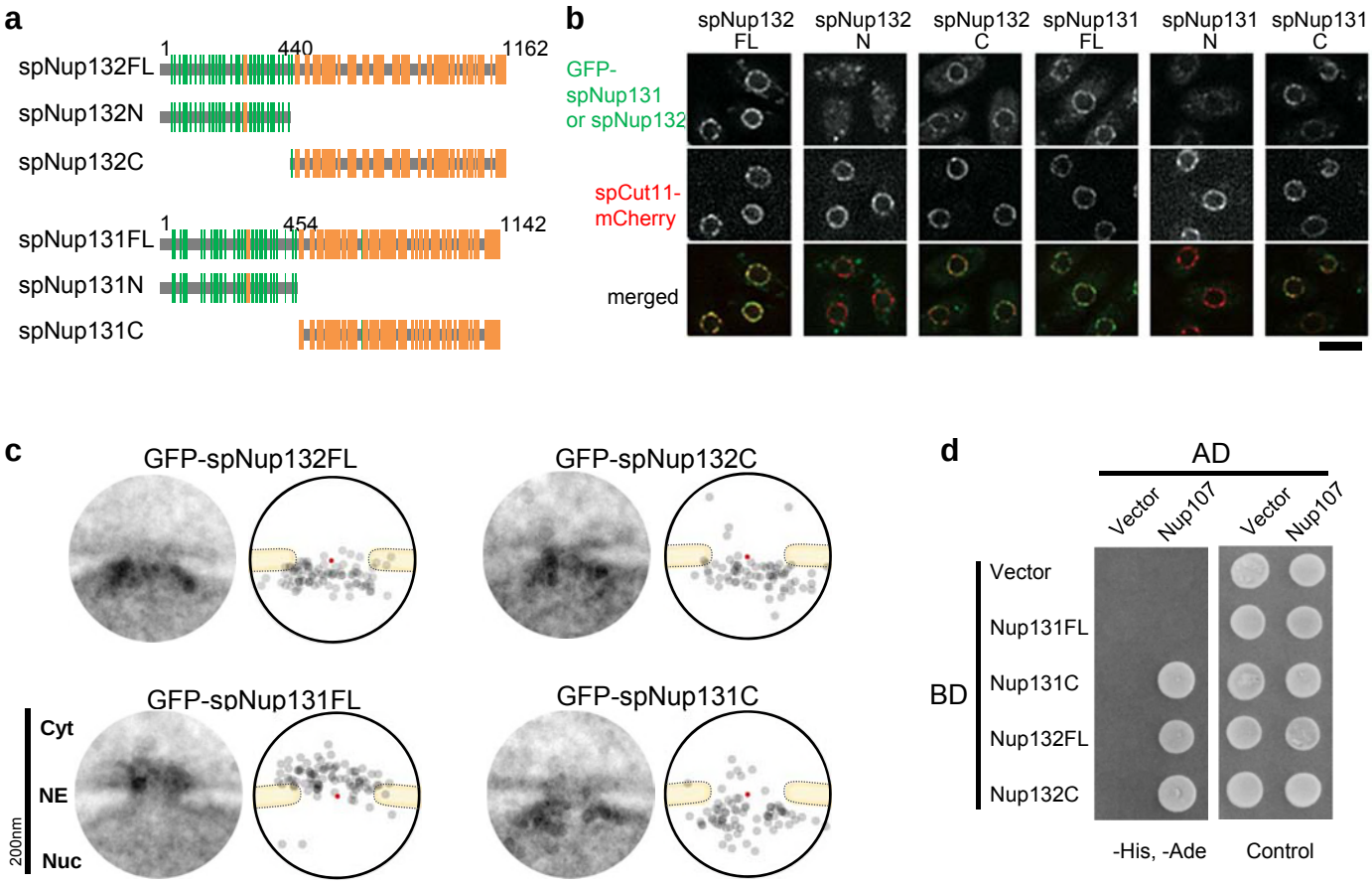

Asakawa et al. Figure 7

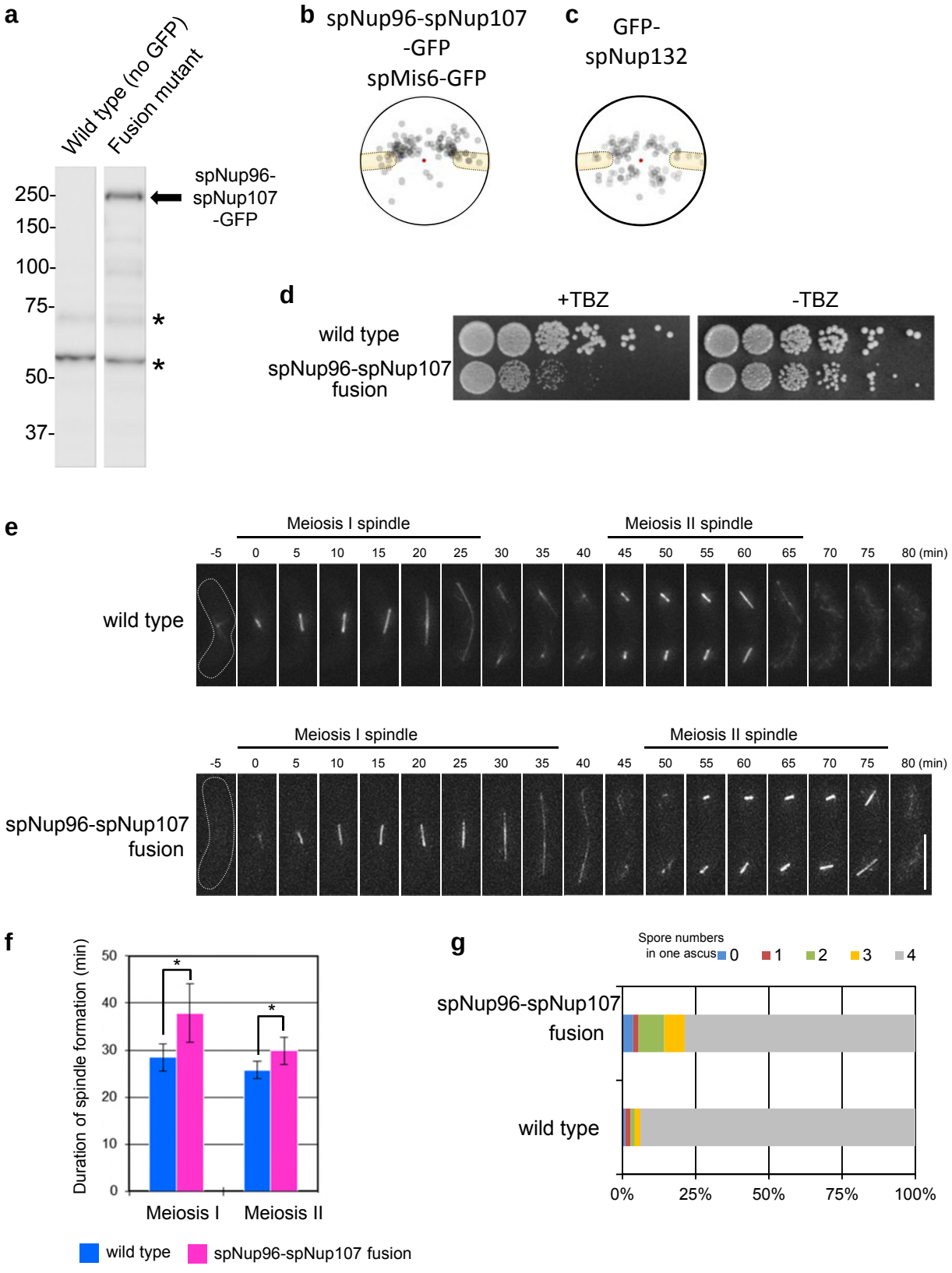

Asakawa et al. Figure 8